ABSTRACT

Title of Thesis: TRANSIENT THERMAL MODELING OF A
                                    RAPID SINTERING PROCESS IN A
                                    NATURAL GAS PIPE ENVIRONMENT

                                    Destiny Oparaocha, Master of Science, 2021

Thesis Directed By: Dr. Paul Albertus, Department of Chemical and
                                    Biomolecular Engineering

The rapid sintering process of a steel paste (steel powder and polyvinylpyrrolidone binder

mixture) onto the interior of an existing pipeline will provide structural reinforcement to

natural gas pipelines, thus enabling pipeline rehabilitation. Methods currently exist for

sintering metal powders. However, metal powder sintering within a pipeline is not typically

addressed. The goal of this study was to develop a model to determine the optimal applied

power and sintering time for a rapid sintering process of steel paste within 30 seconds. A

two-dimensional transient, axisymmetric model simulated the sequential sintering of steel

paste onto the interior of a 30-centimeter (O.D.) by 5-meter steel pipe, with nitrogen gas as

the cooling agent. The steel paste exceeded the minimum target temperature of 1400 °C.

However, full sintering within 30 seconds was unachievable. Further work on identifying

the roles of conduction, convection, and radiation would lead to a more accurate sintering

model.

TRANSIENT THERMAL MODELING OF A RAPID SINTERING PROCESS IN A
NATURAL GAS PIPE ENVIRONMENT

by

Destiny Oparaocha

Thesis submitted to the Faculty of the Graduate School of the
University of Maryland, College Park, in partial fulfillment
of the requirements for the degree of
Master of Science
[2021]

Advisory Committee:
  Professor Paul Albertus, Chair
  Professor Ganesh Sriram
  Professor Dongxia Liu

Acknowledgements

I would like to thank my advisor, Dr. Paul Albertus, for his expertise and support throughout my research process. Thank you for giving me the freedom to explore computation modeling in the energy field, an area that I have always been extremely interested in. Throughout this experience, I finally understood how to synthesize my passion for chemical engineering that I developed as an undergraduate student with my passion for systems engineering.

I am extremely grateful for all of the software assistance that I received from Nathan Brenner Johnson. When I first began my research, I did not have any previous knowledge on COMSOL, which was the modeling software that I used extensively throughout this study. Nathan was such an amazing, patient teacher who helped me to learn valuable COMSOL skills that were critical to the success of my research.

Finally, I would like to thank my family members for all their support throughout my entire educational process, and I would especially like to thank my mom. She has devoted herself to my education for the last two decades, and I would not have achieved all of the incredible milestones in my life without her.

Table of Contents

List of Tables

List of Figures

Chapter 1: Introduction

1.1. Background on REPAIR

The system of interest is a natural gas pipe, as described in the REPAIR (Rapid Encapsulation of Pipelines Avoiding Intensive Replacement) program, which is a program of the U.S. Department of Energy's Advanced Research Projects Agency-Energy (ARPA-E) organization that was initiated in 2020.[1] The goal of REPAIR is to reduce the cost of natural gas distribution pipeline replacement from $1 − 10 million per mile to $500k − $1 million per mile by utilizing pipe-in-pipe coating technology to rehabilitate existing pipelines.[1] In addition to cost reduction, rehabilitation solves the issue of repairing pipelines that are not easily accessible. The typical pipeline replacement process involves the excavation of the existing pipelines and the restoration of the surrounding land, which account for a large fraction of the replacement cost.[1] Excavation and restoration can be difficult to perform in highly congested areas and inconvenient locations, such as natural gas pipes located under major roads.[2] Rehabilitation will eliminate these difficulties.

To rehabilitate pipes, a new pipe will be constructed inside of the original pipe at a target rate of 15 m/hr.[3], such that the original pipe no longer has to be relied on for structural support.[1] Using the appropriate tools, a structural coating (which may be a composite or a single material, such as the steel that is a focus of this thesis) will be deposited onto the interior of the original pipe, and this coating may or may not bind to the surface. Binding may not be necessary or possible if the original inner surface of the pipe

is covered in rust or other contaminants. The coating thickness must be relatively thin so that the inner diameter of the pipe is not significantly decreased. A very thick coating could reduce the delivery capacity of natural gas.[1]

1.2. Thesis Focus

The rapid sintering process of a steel paste (steel powder and polyvinylpyrrolidone binder mixture) onto the interior of an existing pipeline will provide structural reinforcement to natural gas pipelines, thus enabling pipeline rehabilitation. The pipe system addressed by the REPAIR program consists of several components and personnel that must coordinate for the system to be successful.[3] Within this program, there is a "System Components" category that is composed of robots, composites, integrity tools, and data visualization/management.[3] For the purpose of this study, the focus was on the robots and composites elements of the "System Components". The goal of this study was to develop a model to determine the optimal applied power and sintering time (robot parameters) for a rapid sintering process of steel paste (composite) to a target temperature of 1400 °C within 30 seconds. The target temperature was the approximate melting point of the paste. A sintering time of 30 seconds or less would allow our sintering process to meet the target rate of 15 m/hr.[3] Additionally, this sintering time would produce a more energy efficient process than a higher sintering time, such as 5 minutes. The longer the sintering time, the more heat will be lost through conduction in the radial and axial directions as well as heat that will be carried away by nitrogen gas.

1.3. Literature Review

1.3.1. A general method to synthesize and sinter bulk ceramics in seconds

To understand the general principles of a rapid sintering process, a recently published paper from the UMD Liangbing Hu group, *A general method to synthesize and sinter bulk ceramics in seconds,* was reviewed. Methods for a rapid sintering process for ceramic pellets currently exist, and Wang et al. concluded that radiative heating and conduction can be used in an Ultrafast High-Temperature Sintering (UHS) process to generate ceramic materials with a sintering time of 10 seconds.[4] Radiation and conduction were the heat transfer methods used to synthesize and sinter a ceramic pellet.[4] During this process, the ceramic pellet was inserted between two Joule-heating carbon strips, and these strips could heat to a temperature up to 3000°C by the passage of electrical current.[4] The UHS process consisted of 3 steps: 1) 30 second rapid heating to ramp the temperature of the heating element from room temperature to the desired sintering temperature, 2) 10 second isothermal sintering, and 3) 5 seconds of rapid cooling.[4] Wang et al. also called attention to how the physical properties of the pellet, such as density, changed throughout the sintering process.[4] For instance, as the ceramic pellet sintered, it become more dense.[4]

Unlike the sintering process presented in this article, heating can only occur on one side of the steel paste in a pipe environment as opposed to both sides. A heating element can only be placed on the paste surface facing the interior of the pipe. Given that heating only occurs on one side, the sintering time may have to be increased from the suggested 10 seconds to compensate for the lack of a heating element on both sides of the sample. Additionally, sintering on one side of the paste raises the concern of large temperature

3

gradients within the paste. While the general UHS process (raising the temperature of the heating element to a specific temperature, sintering, and cooling) was applicable to our study, some modifications were required. Since sintering within a pipe occurs in a closed environment, heat cannot easily dissipate into the surroundings. This raises the concern of the interior of the pipe reaching a very high temperature, which could potentially damage any inline robotic tools and present safety and environmental concerns. Therefore, a cooling step would have to be consistently applied throughout the UHS. Similar to this article, changes in thermal and physical properties as a function of temperature for the paste layer should be taken into consideration. While the rapid sintering process was addressed, rapid sintering within a pipeline environment with a metal composite was not addressed in this article. However, the general UHS process was applicable to our study.

1.3.2. Supplementary Materials for a general method to synthesize and sinter bulk ceramics in seconds

Supplementary material for the aforementioned journal was evaluated to gain additional knowledge on the UHS process for ceramic pellets. One primary area of interest within the supplementary material was the numerical model for temperature distribution in the ceramic pellet during heating.[5] In this model, the focus was on a 1 mm thick ceramic pellet.[5] The temperature of carbon heaters linearly increased from 22 °C to 2000 °C in 10 or 30 seconds.[5] A 10 second temperature hold at 2,000 °C followed the temperature ramping.[5] In addition to these parameters, material properties such as specific heat capacity, thermal conductivity, density, absorbance, and reflectance were integrated into

the model.[5] Based on the results generated from the model, a more uniform temperature distribution in the pellet could be achieved by slowly ramping the heat for 30 seconds.[5]

Several parameters and conditions from the numerical model should be incorporated into our model. A steel paste layer of 1 mm was determined to be a suitable starting point for thickness. Our model should also utilize a method to heat and hold the temperature for a desired amount of time, and the effects of radiation should be considered in the form of absorbance and reflectance. Regarding the steel paste, some heat will be absorbed at the boundary (absorbance), some heat will pass through the paste (transmittance), and some heat will radiate back from the surface (reflectance). From the numerical model results, it appears that there is a trade-off between sintering time and the uniformity of temperature distribution. While rapid sintering may be desirable from a scheduling perspective, the rapid nature of the sintering process may have to be sacrificed to achieve a more uniform layer.

1.3.3. Rapid Synthesis and Sintering of Metals from Powders

To understand the Ultrafast High-Temperature Sintering (UHS) process within the context of metal powders, which was the material of interest within our study, *Rapid Synthesis and Sintering of Metals from Powders*[6] was reviewed. In addition to rapid sintering methods for ceramic pellets, methods for a rapid sintering process are also available for metal powders. Wang et al. determined that an UHS process could also be used to sinter metal powders that have been pressed into pellets in a matter of seconds with a temperature between 1000 °C and 3000 °C.[6] Similar to the sintering technique used on

ceramic pellets, two Joule-heating carbon heaters were used in a 3 step process to raise the temperature of the heating element to a specific temperature, sinter the metal pellet, and finally cool the metal pellet.[6] It is important to note that the metal powders do not have to be completely melted for the UHS process to be effective. Wang et al. demonstrated that UHS was effective on metals with very high melting points (greater than 2000 °C) as well as powders that contained components with varying melting points.[6] The results indicate that the sintering temperature can be lower than the melting point of the powder. Within this sintering process, the controlled parameters were sintering time and the target sintering temperature.[6]

In our model, the parameters of interest should be closely related to sintering time and temperature. Additionally, the heating element must reach a very high temperature, but this temperature does not have to exceed the melting point of steel. The same concerns from UHS with ceramic pellets, such as extended sintering time due to heating on one side of the paste and the risk of overheating the interior of the pipe, were still present in metal paste sintering. While the rapid sintering process and the use of a metal powder was addressed, rapid sintering within a pipeline environment was not discussed in this article. However, the Wang et al. findings provide confidence that rapid sintering of a steel paste is possible.

1.3.4. Additional References

In addition to the references that were discussed above in detail, other relevant work has focused on the general challenges and approaches to pipeline rehabilitation[7], [8], [9], [10] and the sintering of metal powders to dense metals.[11], [12], [13], [14]

Chapter 2: Methodology

2.1. Model Overview

To achieve structural reinforcement, we considered a 3 mm layer of steel paste sintered to the interior of the existing steel pipe. Due to the low thermal conductivity of the steel paste, a layered approach was used to ensure that the paste was fully sintered. One layer of paste will be sintered 1 mm at a time, with a final thickness of 3 mm. This study focused on analyzing the sintering process of the initial 1mm layer of paste that was sintered onto the interior of the pipe, which is described below in Figure 2.1-1. Figure 2.1-1.a below illustrates the initial and final states of the paste during the sintering process with the associated target temperature (1400 °C) and target sintering time (30 s). Figure 2.1-1.b below depicts the final sintered product (new steel pipe) onto the interior of the existing pipe (old pipe). A two-dimensional transient axisymmetric model was developed in COMSOL to simulate the sequential sintering of steel paste onto the interior of a 30-centimeter (O.D.) by 5-meter steel pipe, with nitrogen gas as the cooling agent. Nitrogen could be introduced to the pipe via on-site nitrogen gas cylinders, as sintering with natural gas in the pipe could pose safety concerns. A sequential heating method was meant to mimic the sintering process of a robotic system. Transient heating occurred in sections axially along the inner surface area of the pipe. The model was then solved using the Finite Element Method (FEM).
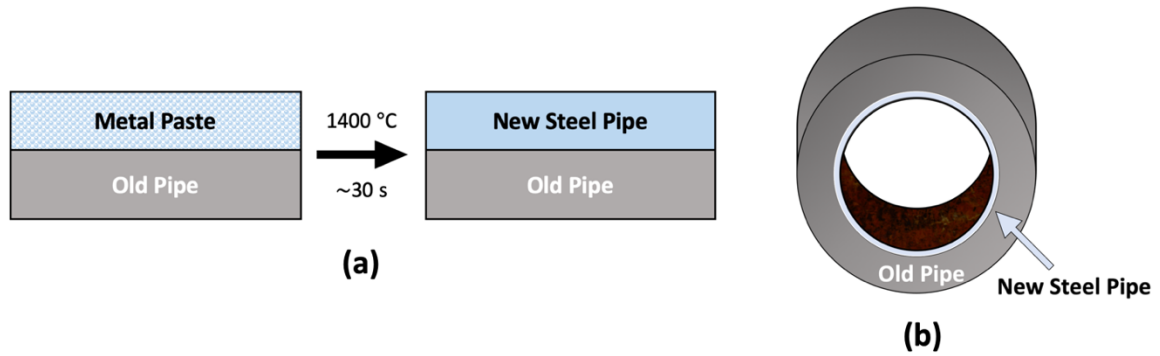
Figure 2.1-1: Overview of the sintering process. (a) Transition from the initial to the final state of the sintering process with the target sintering temperature (1400 °C) and target sintering time (30 s). (b) Final sintered product (new steel pipe) on the interior of the existing pipe (old pipe). Please note that this figure was adapted from the figure on slide 2 of a presentation that was delivered by the Liangbing Hu Group from the University of Maryland, College Park.[15]

Sintering could potentially occur through two different scenarios: 1) Boundary Heating and 2) Radiative Heating. Preliminary findings suggest that radiative heating requires a longer sintering time compared to boundary heating. Although boundary heating occurs more quickly, it may be advantageous to use radiative heating to avoid direct contact between the heating element and the paste layer. Complete surface to surface contact may be difficult if the existing pipes are not thoroughly cleaned and free of rust and debris before the sintering process begins. However, given a lack of information on the radiative properties of the paste, such as emissivity, and the proper orientation of the heater, radiative heating was not considered. As a result, this study focused on the boundary heating scenario, with conduction and convection as the primary methods of heat transfer. Conduction occurred when heat was transferred from the boundary heat source to the paste layer and then into the pipe and surrounding soil. Convection occurred when heat was transferred from the hot paste layer to the flowing nitrogen gas.

Figure 2.1-2 below summarizes the geometric parameters, materials, and heat transfer equations that were used in the model. All geometric parameters are defined below in Table 2.3.1-1, all materials are defined below in Table 2.3.2-1, and all heat transfer equations are defined below in Table 2.3.3-3.
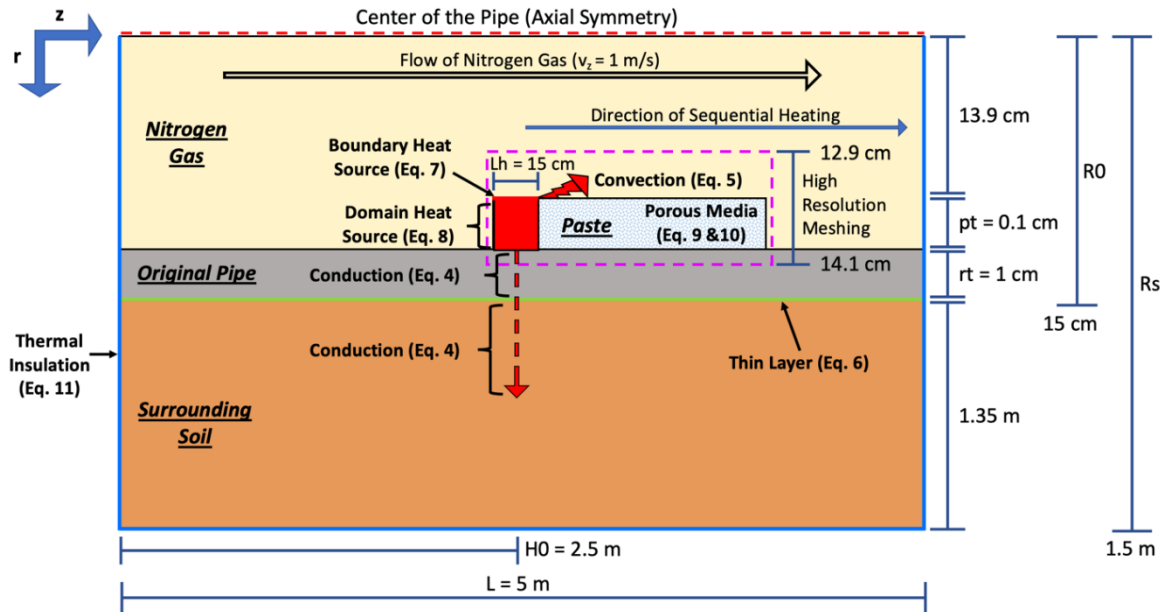
Figure 2.1-2: Summary of the geometric parameters, materials, and heat transfer mechanisms of the pipeline environment. All geometric parameters are defined below in Table 2.3.1-1, all materials are defined below in Table 2.3.2-1, and all heat transfer equations are defined below in Table 2.3.3-3

2.2. Assumptions & Definitions

A two-dimensional transient axisymmetric model was developed in COMSOL with the following assumptions and conditions:

- The flow of natural gas in the pipe was shut off during sintering.

- Nitrogen gas acted as a cooling agent and constantly flowed through the pipe at 1 m/s during the sintering process. The nitrogen gas had a pure plug flow (uniform velocity

10

profile) with a single velocity component in the axial direction. Heat could diffuse to the center of the nitrogen gas, but there was no gas expansion.

- A heater was defined as a section of paste along the nitrogen gas/paste boundary where power was applied. The heater covered $\theta = 0$ to 2π for the specified axial length.

- Each heater only had two positions: 1) "on" and 2) "off". When the heater was "on", a given number of kW (applied power) was constantly generated by the heater. When the heater was "off", the applied power was set to 0 kW.

- Applied power was defined as the amount of power (in kW) that was constantly generated by the heater when it was in the "on" position. The total applied power was defined as the sum of power applied at the nitrogen gas/paste boundary and the power applied throughout the paste.

- Sintering time was defined as the length of time (in seconds) that a heater was generating power.

- Heat was equally absorbed at the surface of the paste facing the interior of the pipe (nitrogen gas/paste boundary) and transmitted through the paste. Therefore, absorbance and transmittance were both 50%. We emphasize this is an important assumption and that when more empirical data is available that allows a more accurate determination of the actual ratio, the model should be updated.

- The steel paste was a porous metal paste (constant porosity of 20%) that consisted of 97% (wt%) 316 stainless steel (SS316) and 3% (wt%) binder, which was polyvinylpyrrolidone (PVP).

- Data on the density (ρ), heat capacity (Cp), and latent heat for SS316 as a function of temperature was retrieved from the Wei Xiong Group at the University of Pittsburgh, College Park. See Appx. A.1, A.2, and A.4 for tabulated values.

- The material properties of PVP remained constant throughout the sintering process.

- The heat capacity of the paste was 97% (wt%) of $Cp_{steel}(T)$ and 3% (wt%) of Cp_{PVP}.

- The density of the paste was 97% (wt%) $\rho_{steel}(T)$ and 3% (wt%) ρ_{PVP}.

- A phase change occurred in the paste layer from 1300 °C to 1425 °C to simulate a porous to solid phase transformation. This range was determined from the solid fraction graph in Appx. A.3.

2.3. Model Set-Up

2.3.1. Geometry

The natural gas pipeline environment was represented by four distinct rectangular domains within a two-dimensional axisymmetric model in COMSOL. Beginning on the left side of Figure 2.3.1-1.b, the four domains are: 1) Nitrogen Gas (yellow), 2) Paste (pink), 3) Original Pipe (green), and 4) Soil (grey). Figure 2.3.1-1.b shows a high-resolution image of the area boxed in red from Figure 2.3.1-1.a.
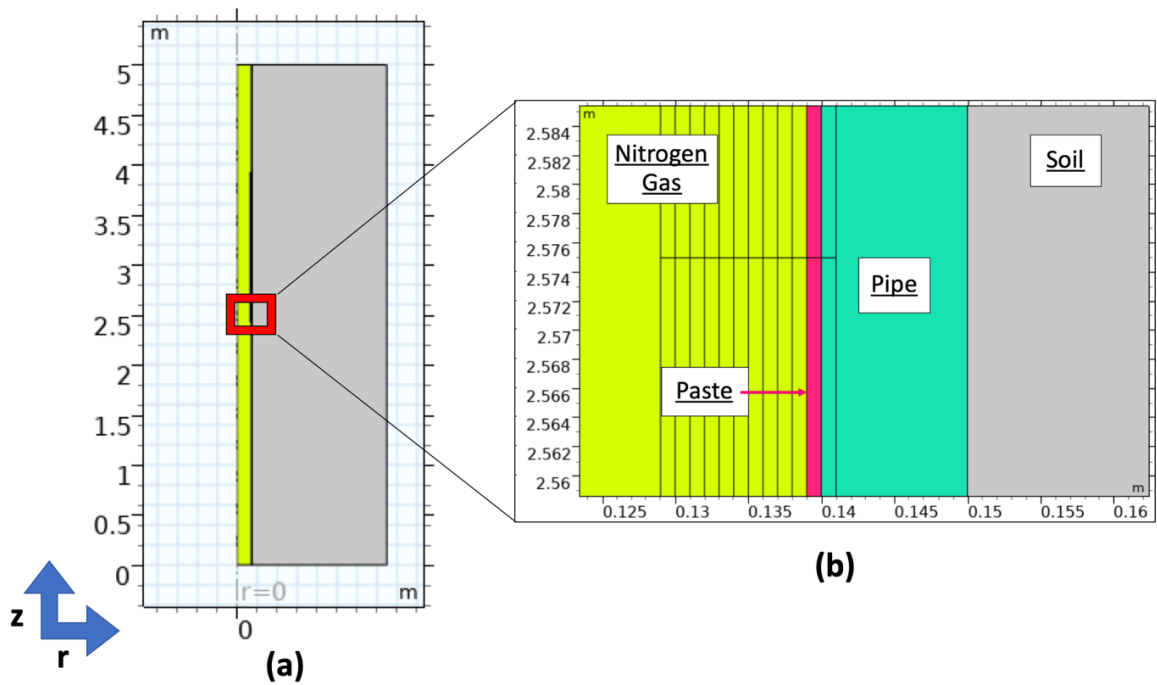
Figure 2.3.1-1: Geometry overview with Nitrogen Gas (yellow), Paste (pink), Original Pipe (green), and Soil (grey). (a) Overview of the geometry for all domains. (b) High resolution image for the area boxed in red from image (a).

All parameters required to establish the geometry of the model are shown below in Table 2.3.1-1.

Table 2.3.1-1: Geometric Parameters

Parameter Name	Value/ Expression	Unit	Parameter Description
r0	0	N/A	Initial r position of the gas domain
z0	0	N/A	Initial z position of the gas domain
L	5	m	Total length of the pipe
Ro	15	cm	Outer pipe radius
rt	1	cm	Thickness of the pipe
Rs	1.5	m	Distance from the center of the pipe to the edge of the soil
Lh	15	cm	Length of each heater
pt	0.1	cm	Paste thickness
H0	L/2	cm	Axial location of the first heater
High_m	1	mm	Thickness of each high-resolution region for meshing

This geometry set-up represented a steel pipeline that was located underground beneath a layer of soil with nitrogen gas flowing through the interior of the pipe. A steel paste layer was added onto the interior of the pipe. This paste layer was equally divided into 10 sections such that each section could be sintered individually. Each section was then assigned a separate heater with specific heat transfer mechanisms (described below in 2.3.3. Heat Transfer Mechanisms), resulting in a total of 10 heaters. The center of the first section began at 2.5 m (axially) in the pipe. Given that most of the heat transfer occurred near the paste layer, it was determined that a higher resolution of mesh would be required in that region in order to properly resolve steep thermal gradients. The high-resolution mesh areas were represented as arrays of rectangles that aligned with the 10 sections of

paste. These 1 mm thick rectangles were added in 1 mm increments 1 cm into the nitrogen gas domain from the nitrogen gas/paste boundary and 1 mm into the pipe domain from the paste/pipe boundary. As a result, there was a 10 by 10 array (1.5 m by 1 cm) of a high-resolution area in the nitrogen gas and a 10 by 1 array (1.5 m by 1 mm) of a high-resolution area in the pipe.

2.3.2. Materials and Material Properties

Each domain (nitrogen gas, paste, original pipe, and soil) was represented with a different material, which is depicted below in Table 2.3.2-1. Each material required the thermal conductivity, specific heat capacity, density, and ratio of specific heats to be specified. Some materials, such as Nitrogen Gas and Steel AISI 4340, were predefined materials in COMSOL, while other materials, such as the paste and soil, had to be manually defined.

Table 2.3.2-1: Materials and material properties for the gas, paste, pipe, and soil domains

Domain	Material	Thermal Conductivity (k) $\left[\dfrac{W}{m*K}\right]$	Specific Heat Capacity (Cp) $\left[\dfrac{J}{kg*K}\right]$	Density (ρ) $\left[\dfrac{kg}{m^3}\right]$	Ratio of Specific Heats (γ)
Gas	Nitrogen Gas - v_z = 1 m/s - v_r = 0 m/s - P_{abs} = 20 psi	COMSOL Built-In Function	COMSOL Built-In Function	COMSOL Built-In Function	1.4[16]
Paste	Paste - 97% (wt%) SS316 - 3% (wt%) PVP - Porosity = 20%	1.42[17]	$Cp_{powder}(T) = 0.97 Cp_{steel}(T) + 0.03 Cp_{PVP}$	$\rho_{power}(T) = \left[\dfrac{0.97}{\rho_{steel}(T)} + \dfrac{0.03}{\rho_{PVP}}\right]^{-1}$	1
	SS316 - MW = 0.054 kg/mol[8]	15[18]	$Cp_{steel}(T)$ (Appx. A.2)	$\rho_{steel}(T)$ (Appx. A.1)	N/A
	PVP	N/A	1542[19]	1200[20]	N/A
Pipe	Steel AISI 4340	44.5	475	7850	1
Soil	Saturated Silty Soil - Volume Ratio (soil:water) = 5:5	1.4[21]	1480[22]	1350[21]	1

2.3.3. Heat Transfer Mechanisms

"Heat Transfer in Solids and Fluids" was the primary heat transfer module used in COMSOL. All domains began at an initial temperature of 10 °C (a reasonable ground temperature), and axial symmetry existed at the center of the pipe. Through conduction, heat transfer occurred in the solid domains (pipe and soil). In the fluid domain (nitrogen gas), convection caused heat to transfer from the hot paste to the nitrogen gas, which flowed axially at 1 m/s. A thin layer was applied to the pipe/soil boundary to account for the drastic difference in the material properties of the pipe and soil domains as well as to ensure continuity between the two domains. A nonlayered shell with a thickness of 10^{-4} m and a thermally thin approximation was applied to the thin layer. The material properties of the thin layer were the same properties as those of the pipe domain. Furthermore, thermal insulation existed on the edges of the model, and an edge was represented as a line that passed through a set of (r, z) coordinates. The following sets of coordinates (with units of meters) represented the edges where thermal insulation was defined in the model: (0,0) to (1.5, 0), (1.5,0) to (1.5, 5), and (1.5, 5) to (0, 5).

The "Porous Medium" module was used to define heat transfer within the paste, which was a porous domain. The porous matrix utilized the material properties of the paste. A phase change occurred in the fluid of the porous medium from 1300 °C to 1425 °C to more accurately represent the sintering process. In reality, the porous paste layer would transition to a solid layer during sintering. To simulate this transition, the thermal conductivity of the paste transitioned from the initial paste thermal conductivity (1.42 W/(m·K)) to the thermal conductivity of SS316 (15 W/(m·K)). The heat capacity and

density of the paste changed accordingly as a function of temperature throughout the 1300 °C to 1425 °C phase change interval. The latent heat as a function of temperature (Appx. A.3) was also incorporated into the phase change.

To account for absorbance and transmittance within the paste layer, two separate heat sources were used: 1) Boundary Heat Source and 2) Domain Heat Source. To mimic 50% absorbance and 50% transmittance, heat was equally absorbed at the nitrogen gas/paste boundary (boundary heat source) and transmitted via a volumetric heat source with uniform heat generation throughout the paste layer (domain heat source) . Each heater was represented by individual sets of boundary and domain heat sources. All boundary and domain heat sources only consisted of two states: 1) "on" and 2) "off". When a heater was turned on, a constant power was applied to increase the temperature of the boundary and domain. When the heater was turned off, the power applied to the boundary and domain was switched to 0 kW. Boolean expressions were used to assign a heat rate to the boundary and domain of each heater to simulate the sequential heating of the paste layer in the axial direction. The Boolean expressions allowed for a heat rate to be applied for a given sintering time during a specific time interval in the simulation. All Boolean expressions are described below in Table 2.3.3-1. Please note that the "Equation Group #" is only used to organize the equations in this thesis. All variables used in Table 2.3.3-1 are described below in Table 2.3.3-2.

Table 2.3.3-1: Boolean expressions for power used in the domain and boundary heat source modules.

Equation Group #	Heater (n)	Equation(s)
1	1	$P_{b,n=1} = P_{0,n=1} =$ $P_i * (t \geq 0 \text{ \&\& } t \leq ST_1) + 0 * ! (t \geq 0 \text{ \&\& } t \leq ST_1)$
2	2	$P_{b,n=2} = P_{0,n=2} =$ $P_i * (t \geq ST_1 \text{ \&\& } t \leq ST_1 + ST_2) + 0 \\ * ! (t \geq ST_1 \text{ \&\& } t \leq ST_1 + ST_2)$
3	3 – 10	$P_{b,n\geq3} = P_{0,n\geq3} =$ $P_i * (t \geq ST_1 + ST_2 + (n-3) * ST_3 \text{ \&\& } t \\ \leq ST_1 + ST_2 + (n-2) * ST_3) \\ +0 * ! (t \geq ST_1 + ST_2 + (n-3) * ST_3 \text{ \&\& } t \\ \leq ST_1 + ST_2 + (n-2) * ST_3)$

Table 2.3.3-2: Summary table for all variables used in the equations in Table 2.2.3-1 above.

Notation	SI Unit	Description
$P_{b,n}$	W	Heat rate, boundary heat source of heater n
$P_{0,n}$	W	Heat rate, domain heat source of heater n
P_i	W	Constant applied power
n	dimensionless	Heater number
ST_n	s	Sintering Time for heater n
t	s	Time (output time)
&&	dimensionless	Boolean operator for "AND"
!	dimensionless	Boolean operator for "NOT"

All heat transfer mechanisms were represented through a variety of partial differential equations, which were solved in COMSOL with the Finite Element Method (FEM). All equations used during heat transfer were built into the COMOL heat transfer modules. Table 2.3.3-3 below summaries the heat transfer equations used to solve the model. All variables used in Table 2.3.3-3 are defined below in Table 2.3.3-4. Please note

that the "Equation Group #" is only used to organize the equations in this thesis. Additionally, boundary probes were defined at the nitrogen gas/paste and paste/pipe boundaries to determine the maximum temperatures along these boundaries as various time points. These temperature readings were used during parameter optimization, which is described below in section 3.3 Optimized Parameters. A domain probe was also defined at the paste domain for Heater 1 to determine the average temperature of Heater 1 at the end of its sintering time. This temperature reading was used in the energy efficiency calculations, which are described below in section 3.6 Energy Efficiency.

Table 2.3.3-3: Heat transfer equations summary table.

Equation Group #	Domain (D)/ Boundary (B)	Heat Transfer Mechanism	Equation(s)
4	D: Pipe, Soil	Conduction	$\rho C_p \dfrac{\partial T}{\partial t} + \nabla q = 0$ $q = -k\nabla T$
5	D: Nitrogen Gas	Convection/ Conduction	$\rho C_p \dfrac{\partial T}{\partial t} + \rho C_p u \nabla T + \nabla q = 0$ $q = -k\nabla T$
6	B: Pipe/Soil	Thin Layer	$-n \cdot q = -d_s \rho C_p \dfrac{\partial T}{\partial t} - \nabla_t \cdot d_s q_s$ $q_s = -k\nabla_t T$
7	B: Nitrogen Gas/Paste	Boundary Heat Source	$-n \cdot q = Q_b$ $Q_b = \dfrac{P_b}{A}$
8	D: Paste	Domain Heat Source	$Q = Q_0$ $Q_0 = \dfrac{P_0}{V}$
9	D: Paste	Porous Media, Fluid, & Matrix	$(\rho C_p)_{eff} \dfrac{\partial T}{\partial t} + \nabla q = Q$ $q = -k_{eff}\nabla T$ $(\rho C_p)_{eff} = \theta_s \rho_s C_{p,s} + \epsilon_p \rho_f C_{p,f}$ $k_{eff} = \theta_s k_s + \epsilon_p k_f + k_{disp}$ $k_s = \dfrac{k_b}{\theta_s}, \rho_s = \dfrac{\rho_b}{\theta_s}, C_{p,s} = \dfrac{C_{p,b}}{\theta_s}$
10	D: Paste	Phase Change	$\rho_f = \theta_1 \rho_1 + \theta_2 \rho_2$ $C_{p,f} = \dfrac{1}{\rho}\left(\theta_1 \rho_1 C_{p,1} + \theta_2 \rho_2 C_{p,2}\right)$ $+ L_{1\to2} \dfrac{\partial \alpha_m}{\partial T}$ $\alpha_m = \dfrac{1}{2}\left(\dfrac{\theta_2 \rho_2 - \theta_1 \rho_1}{\theta_1 \rho_1 + \theta_2 \rho_2}\right)$ $k_f = \theta_1 k_1 + \theta_2 k_2$ $\theta_1 + \theta_2 = 1$
11	Edges of the model	Thermal Insulation	$-n \cdot q = 0$

Table 2.3.3-4: Summary table for all variables used in the equations in Table 2.3.3-3 above. Please note the Notation, SI Unit, and Description were taken from the Heat Transfer Module User's Guide for COMSOL Multiphysics v. 5.4.[23]

Notation	SI Unit	Description
ρ	kg/m^3	Density
C_p	J/(kg·K)	Specific heat capacity at constant pressure
T	K	Temperature
t	s	Time (output time)
q	W/m^2	Conductive heat flux
Q	W/m^3	Heat source
u	m/s	Fluid velocity vector
∇	dimensionless	Gradient operator
n	dimensionless	Normal vector toward exterior
d_s	m	Thickness of shell or thin layer
∇_t	dimensionless	Tangential gradient operator
q_s	W/m^2	Conductive heat flux in solid phase
Q_b	W/m^2	Boundary heat source
P_b	W	Heat rate, boundary heat source
A	m^2	Total boundaries area
Q_0	W/m^3	Distributed heat source
P_0	W	Heat rate
V	m^3	Total domain volume
$(\rho C_p)_{eff}$	J/(m^3·K)	Effective volumetric heat capacity at constant pressure
ρ_f	kg/m^3	Density, fluid phase
$C_{p,f}$	J/(kg·K)	Specific heat capacity at constant pressure, fluid phase
Q_{geo}	W/m^3	Geothermal heat source
k_{eff}	W/(m·K)	Effective thermal conductivity
θ_s	rad	Zenith angle of the Sun
ρ_s	kg/m^3	Density, solid phase
$C_{p,s}$	J/(kg·K)	Specific heat capacity at constant pressure, solid phase
ϵ_p	dimensionless	Porosity
k_s	W/(m·K)	Thermal conductivity, solid phase
k_f	W/(m·K)	Thermal conductivity, fluid phase
k_{disp}	W/(m·K)	Dispersive thermal conductivity tensor
θ_i	dimensionless	Volume fraction of phase i in porous media
k_i	W/(m·K)	Thermal conductivity of phase i in porous media

ρ_i	kg/m^3	Density of phase i in porous media
α_m	dimensionless	Vapor mass fraction
$C_{p,i}$	J/(kg·K)	Specific heat capacity at constant pressure of phase i in porous media
$L_{1\rightarrow2}$	J/kg	Latent heat from phase 1 to phase 2
k_b	W/(m·K)	Dry bulk thermal conductivity
ρ_b	kg/m^3	Dry bulk density
$C_{p,b}$	J/(kg·K)	Dry bulk heat capacity at constant pressure

2.3.4. Model Meshing

Mesh was applied to all domains to allow the model to be solved with the Finite Element Method (FEM).[24] As described above in section 2.3.3. Heat Transfer Mechanisms, partial differential equations (PDEs) were used to describe the physics of the model. However, these PDEs could not be solved with traditional analytical methods. Instead, the PDEs were approximated with discretization methods in numerical model equations.[24] Meshing the model defined the discretization of each domain, which allowed these PDE approximations to then be computed with the FEM.

The nitrogen gas, paste, pipe, and soil domains were all meshed with "User Controlled Mesh" as the mesh sequence type. All domains used a mesh type of either mapped or free triangular, and the mesh specifications are described below in Table 2.3.4-1. Please note that the notation used in Table 2.3.4-1 below also applies to Figure 2.3.4-1.

23

Table 2.3.4-1: Mesh specifications for all domains/boundaries with the associated mesh type, element size, and mesh distribution.

Notation	Domain (D)/ Boundary (B)	Mesh Type	Element Size	Mesh Distribution	
				Distribution Type	Number of Elements A = Axial R = Radial
1	B: Paste/Pipe	Mapped	N/A	Fixed Number of Elements	A = 160 R = 40 (per 1 mm section)
2	D: Soil	Free Triangular	Finer	N/A	N/A
3	B: Pipe/Soil	Free Triangular	N/A	Predefined; Geometric Sequence (Symmetric distribution)	A = 1000 (Element Ratio = 1)
4	B: Nitrogen Gas/High Resolution Nitrogen Gas	Mapped	N/A	Predefined; Geometric Sequence (Symmetric distribution)	R = 40 (per 1 mm section)
5	B: Nitrogen Gas/Pipe	Free Triangular	N/A	Fixed Number of Elements	A = 500
6	D: Nitrogen Gas, Pipe	Free Triangular	Fine	N/A	N/A
7	B: Nitrogen Gas/Pipe	Free Triangular	N/A	Fixed Number of Elements	A = 200

Once the mesh had been defined for each domain and/or boundary, the mesh of the entire model was built, as described below in Figure 2.3.4-1. In Figure 2.3.4-1, a number followed by an "A" or "R" represents the direction (A = axial or R = radial) that a mesh distribution was applied along a boundary. A number that is not followed by an "A" or "R"

means that the mesh was applied to an entire domain. Once the model mesh was built, the "Mesh Quality" (described below in section 3.1 Mesh Quality) was assessed and a "Convergence Study" (described below in section 3.2 Convergence Study Results) was performed to ensure that the model produced accurate results.
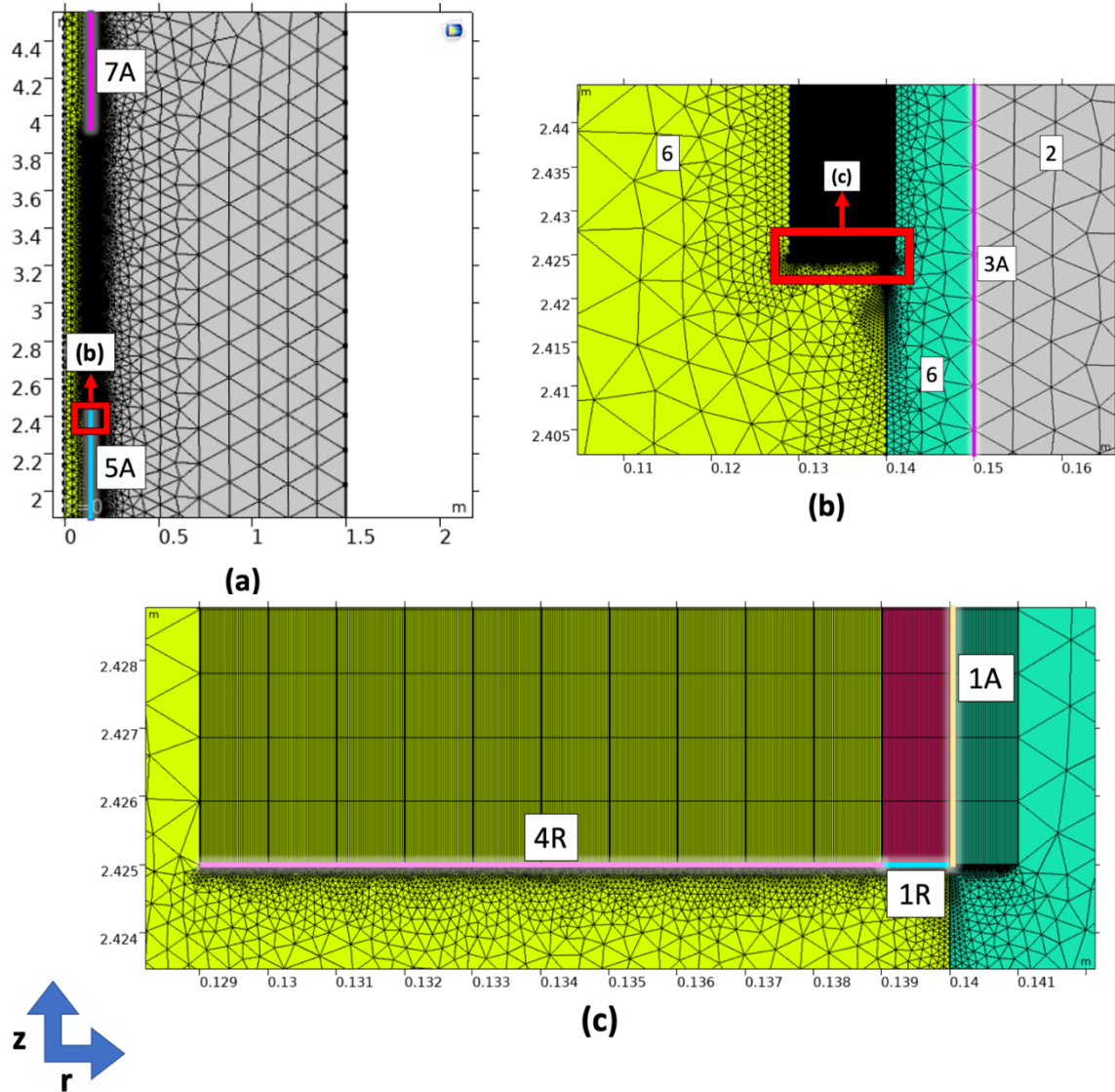
Figure 2.3.4-1: Meshing of all domains using the following notation: B = Boundary, D = Domain, A = Axial, R = Radial, 1 = B: Paste/Pipe, 2 = D: Soil, 3 = B: Pipe/Soil, 4 = B: Nitrogen Gas/High Resolution Nitrogen Gas, 5 = B: Nitrogen Gas/Pipe, 6 = D: Nitrogen Gas, Pipe, and 7 = B: Nitrogen Gas/Pipe. (a) High level mesh image for all domains. (b) High resolution image for the area boxed in red from image (a). (c) High resolution image for the area boxed in red from image (b).

25

2.3.5. Cut-Line Set-Up

Cut-lines were established axially at various domain boundaries to allow the temperature to be measured at these boundaries. Axial cut-lines were used to determine the temperature gradient radially in the paste, from the nitrogen gas/paste boundary to the paste/pipe boundary. As shown below in Figure 2.3.5-1, a total of four axial cut-lines were defined at the interfaces between the different domains.
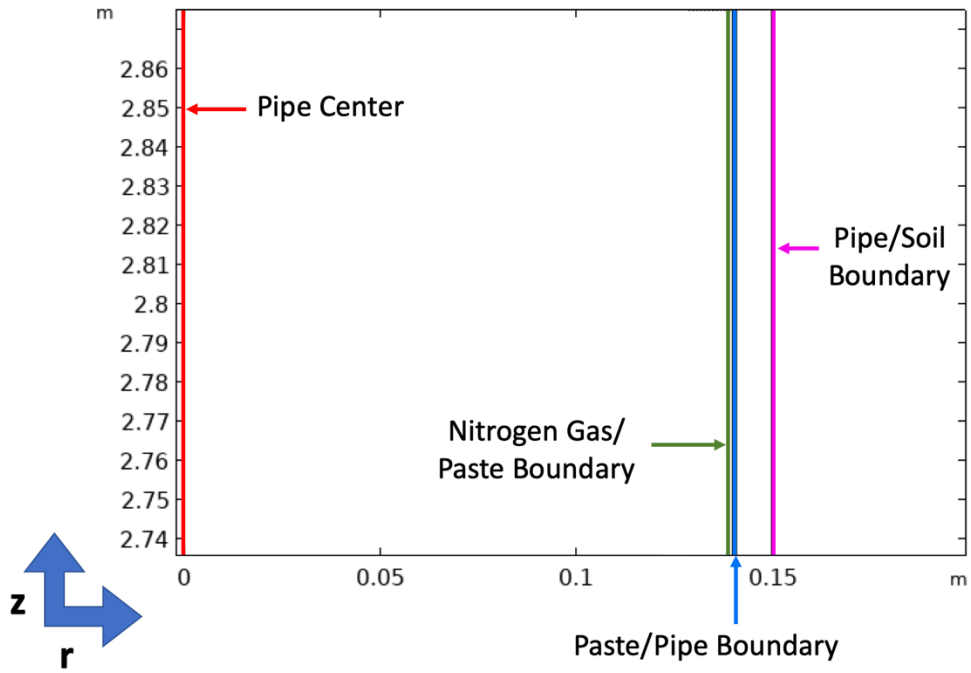
Figure 2.2.5-1: Axial cut-lines at the interfaces between all domains.

Cut-lines were defined radially to determine how the temperature changed from the center of the pipe through the soil. Radial cut-lines, which are described below in Figure 2.3.5-2, were also used to determine temperature gradients axially throughout the paste layer. As shown below in Figure 2.3.5-2.a, there were 10 total radial cut-lines through the center of each heater. As described in Figure 2.3.5-2.b, there were 11 total cut-lines through the boundaries of each heater. 9 cut-lines passed through the interfaces of the 10 heaters,

26

one cut-line passed through the lower edge of Heater 1, and one cut-line passed through

the upper edge of Heater 10.
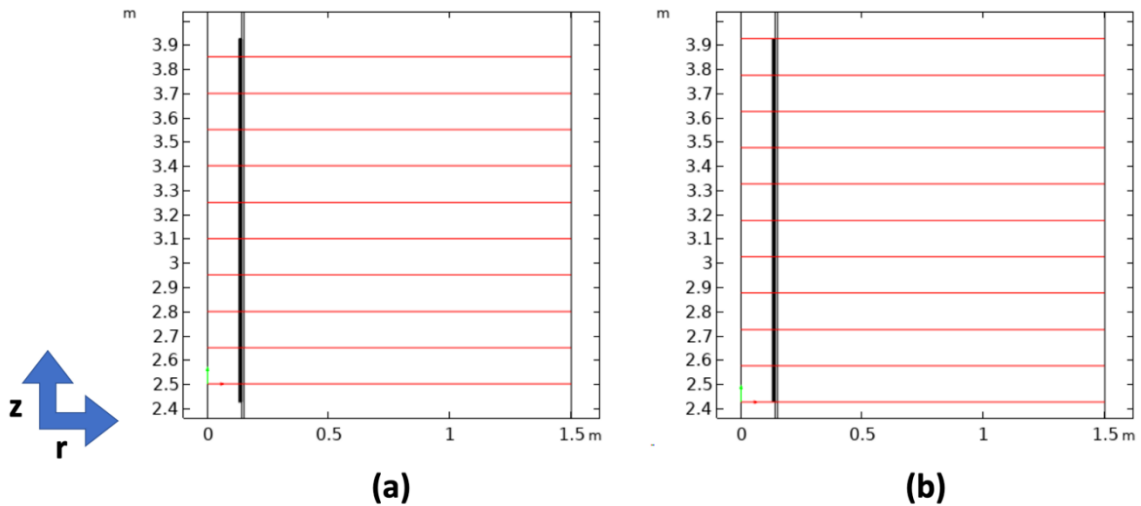
Figure 2.3.5-2: Radial cut-lines. (a) Radial cut-lines through the center of each heater. (b) Radial cut-line through the boundary of each heater.

2.4. Model Execution

2.4.1. Test Case 1: Nitrogen Gas Flow "On"

Various sintering time and applied power combinations were run using the "Parametric Sweep" function in the "Study" module of COMSOL to determine the optimal sintering time and applied power for each heater. These parameters were optimized for each heater individually. Beginning with Heater 1 only (Heater 1 was enabled and Heaters 2 – 10 were disabled), all possible combinations of sintering time from 0 to 90 seconds in 1 second intervals and applied power from 25 kW to 300 kW in 25 kW intervals were run. Since heat would be present in the system after Heater 1, the parameters for Heater 2 would differ from those of Heater 1. Once the optimal parameters were determined for Heater 1,

27

the same parameter combinations were run on Heater 2, with Heater 1 enabled with its optimal parameters and Heaters 3 – 10 disabled. The optimal parameters were then determined for Heater 2. The same process was completed once more on Heater 3 (enable the previous heaters with optimized parameters and disable subsequent heaters). Once the optimal parameters had been determined for Heater 3, the same parameters from Heater 3 were applied to Heaters 4 – 10. Finally, all heaters were enabled with their appropriate parameters. The model was then solved using a "Time Dependent Study" module (without the "Parametric Sweep") with an output time ranging from 0 to SUM(Sintering Times for all Heaters) in 1 second intervals. The key solver settings used during model execution are described below in Table 2.4.1-1.

Table 2.4.1-1: Key Time-Dependent Solver settings

Solver Setting Category	Solver Setting	Solver Setting Value
Time-Dependent Solver	Tolerance Factor	0.1
	Relative Tolerance	0.01
Fully Coupled	Jacobian Update	Once per time step
	Nonlinear Method	Constant (Newton)
	Termination Technique	Tolerance
	Termination Criteria	Solution

For Test Case 1, the temperature profiles were calculated for every time step at various interfaces. Using the axial cut-lines, the temperatures at the center of the pipe, nitrogen gas/paste boundary, paste/pipe boundary, and pipe/soil boundary were calculated. Using the radial cut-lines, the temperatures through the center of the heater and at the boundary of the heaters were calculated.

2.4.2. Test Case 2: Nitrogen Gas Flow "Off"

Test Case 2 was used to determine the impact of nitrogen gas on the temperature inside the pipe. Since heat will be applied to the paste by robotic tools, it was important to ensure that the temperature within the gas did not exceed 45 °C[1] for an extended period of time. To determine the impact of the cooling effects of the nitrogen gas flow, the model was run with all 10 heaters enabled with their respective optimized parameters and the nitrogen gas turned off ($v_{gas,z} = 0$ m/s). Note that the parameters for the heaters were not re-optimized for Test Case 2. Only the temperature at the center of the pipe (using the axial cut-line) was calculated. The same solver settings from Test Case 1 were used in Test Case 2.

2.5. Convergence Study

The purpose of the convergence study was to assess the trade-off between computation time and model accuracy. The accuracy of the model is directly linked to the mesh element size. By decreasing the mesh size of elements, a more refined mesh will be produced. Consequently, a more refined mesh results in a higher number of elements used to solve the model with the FEM, leading to a more accurate solution. As the number of elements increases and approaches infinity, the approximation begins to approach the exact solution. However, a higher refinement of the mesh requires a higher computation time. A good mesh should result in a model solution that is a reasonable approximation of the exact solution within an acceptable margin of error.

---

[1] Based on discussions with my advisor, Dr. Paul Albertus, we determined that 45 °C was approximately the maximum temperature that potential robotic tools used in the sintering process could withstand.

The nitrogen gas/paste boundary was the region of interest for the convergence study because this boundary was the location where the steepest temperature gradients were expected. The convergence study was performed on the nitrogen gas/paste boundary maximum temperature results from Test Case 1. The mesh distributions 1A, 1R, and 4R from Figure 2.3.4-1.c were all changed by a single factor at the same time. The factors used were 0.05, 0.1, 0.125, 0.25, 0.5, and 1. For each factor, the maximum temperatures of each heater at the nitrogen gas/paste boundary were documented, and the solver time was also recorded. The mesh was considered insufficient if the temperature results produced by any of the aforementioned factors differed from the original temperature solution by $\pm1\%$.

Chapter 3: Results & Discussion

3.1. Mesh Quality

A good quality mesh is necessary for the model to produce accurate results. Figure 3.1-1 below depicts the mesh quality for all domains. The green regions (1 on the mesh quality scale) represent a high-quality mesh, which indicates that the correct element (i.e. mapped mesh/free triangular with the appropriate mesh distribution) was chosen. The red regions (0 on the mesh quality scale) represent a low-quality mesh, which indicts that a better mesh element should have been selected. Note that the mesh quality is defined based only on geometric aspects of the modeling domain, boundaries, and the mesh elements.
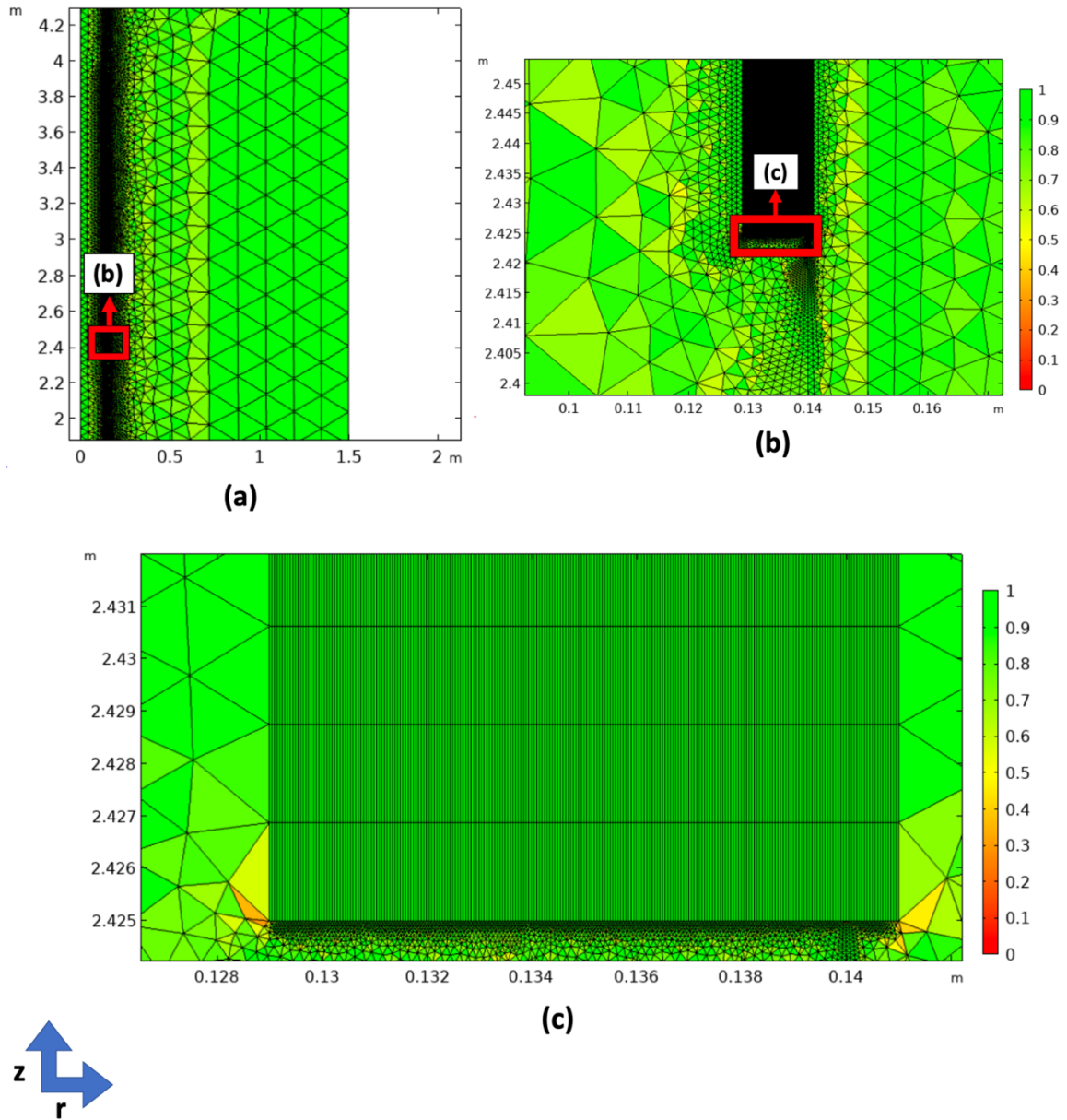
Figure 3.1-1: Mesh quality of all domains. (a) High level mesh quality image. (b) High resolution image for the area boxed in red from image (a). (c) High resolution image for the area boxed in red from image (b).

In Figure 3.1-1.a, the mesh quality appears to be green for all elements, resulting in a mesh quality of 0.7 to 1 for each individual element. In Figure 3.1-1.b, the mesh quality appears to be green for all elements, but there are lighter green areas, which are indicative

of a lower quality mesh. In Figure 3.1-1.c, all elements within the high-resolution mesh region are a dark green, which represents a high-quality mesh. There are a few yellow, lower quality mesh elements present. However, these elements are outside the critical high-resolution mesh region.

According to the Domain Element Statics (located under the "Mesh Statistics" in COMSOL), the average element quality was 0.9855, which was very close to 1. An element quality close to 1 indicates a good quality mesh. Based on the mesh quality plots (Figure 3.1-1.a – Figure 3.1-1.c) and the average element quality statistic, we can say that the mesh quality was "good". However, we could not conclude that our model results were accurate solely based on a "good" mesh quality. Since the mesh quality was only related to the geometric aspects of the model, COMOL did not determine where there were steep temperature gradients, which was critical to our model results. Therefore, a convergence study was necessary to determine how the model solution was influenced by the mesh.

3.2. Convergence Study Results

The results of the convergence study were essential to determining whether our mesh was sufficient for producing temperature profiles along the nitrogen gas/paste boundary, which was the boundary where most of the heat transfer activity occurred in this model. Figure 3.2-1 below describes the results of the convergence study.
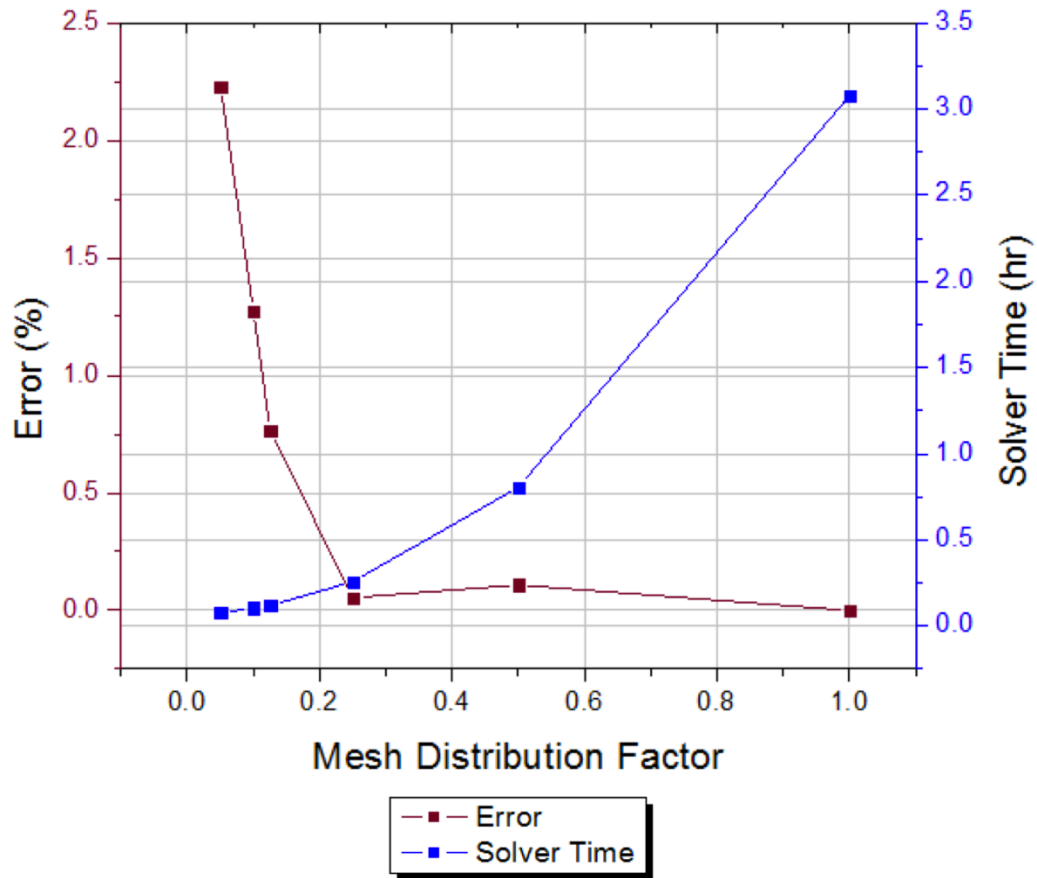
Figure 3.2-1: Mesh convergence study on the average maximum temperature at the nitrogen gas/paste boundary across all heaters for the mesh distribution factors of 0.05, 0.1, 0.125, 0.25, 0.5, and 1.

Figure 3.2-1 shows that a factor of 0.1 results in an error that exceeds 1% while a factor of 0.125 results in an error that is less than 1%. Therefore, a factor of 0.125 or greater would ensure temperature results at the nitrogen gas/paste boundary within the acceptable margin of error. The error begins to stabilize after a factor of 0.25, but the solver time also begins to increase after this point. Therefore, a factor of 0.25 would minimize the error and solver time.

The results imply that a lower resolution mesh could have been used to obtain results within a reasonable margin of error (±1%). A lower resolution mesh would reduce the solver time, which would have been beneficial when running various combinations for optimizing the parameters. Even when the mesh factor was decreased from 1 to 0.25, the solution changed by less than 1%. This study shows that our mesh was sufficient and produced an accurate approximation to the exact solution for the processes modeled.

3.3. Optimized Parameters

Based on the results of the Parametric Sweep for Test Case 1, the optimal parameters for sintering time and total applied power were determined. The optimal parameters were determined by first selecting the sintering time and applied power combinations that resulted in nitrogen gas/paste boundary temperatures of a minimum of 1400 ℃. Then, the paste/pipe boundary temperatures of the selected combinations were analyzed to determine the radial temperature gradient within the paste. The parameter combination with a minimum nitrogen gas/paste boundary temperature of 1400℃ and the smallest temperature gradient was chosen. When assessing the parameter combinations, there was a noticeable trade-off between sintering time, applied power, and temperature gradients. Slower heating (high sintering time) resulted in a more evenly sintered paste layer, but it took longer for the paste to reach the target temperature. Furthermore, a higher applied power would decrease the sintering time, but that led to a higher temperature gradient. The optimal parameters are described below in Table 3.3-1. In Table 3.3-1, total applied power is the sum of the power at the boundary heat source and domain heat source.

Table 3.3-1: Optimal parameters based on Test Case 1.

Heater	Sintering Time (s)	Total Applied Power (kW)
1	85	200
2	55	250
3 – 10	60	250

Based on the sintering time for most of the heaters (Heaters 3 – 10), the linear sintering speed in the axial direction was calculated. Since the sintering time of Heaters 3 to 10 was 60 s and the length of each heater in the axial direction was 15 cm, the linear speed was 15 cm/60s or 9 m/hr. However, this linear sintering speed was only 60% of the target speed of 15 m/hr. The sintering time of the heaters must be reduced to meet the target sintering speed.

3.4. Axial Temperature Profile Results

To analyze the temperature profiles from the axial cut-lines, the maximum temperature of each heater was read to the nearest 1 °C (except for nitrogen gas "on", which was read to the nearest 0.1 °C) in the COMSOL plots. The average maximum temperature across all heaters was then calculated.

3.4.1. Center of the Pipe

Figure 3.4.1-1 below depicts the temperature at the center of the pipe for all time steps with the nitrogen gas flow "on". The maximum temperature at the center of the pipe for each heater with the associated average is described below in Table 3.4.1-1.
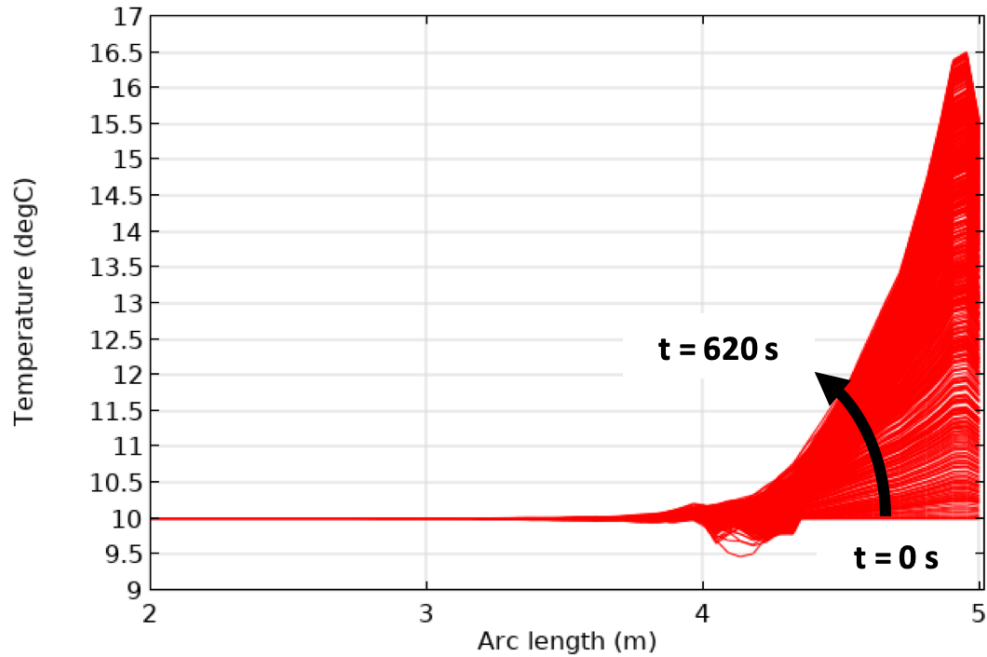
Figure 3.4.1-1: Temperature of the center of the pipe with nitrogen gas flow "on". Each line represents the temperature at the center of the pipe at a specific axial length for each second of the simulation from 0 s to 620 s.

Table 3.4.1-1: Maximum temperature at the center of the pipe for each heater (with nitrogen gas flow "on") with the associated average.

Heater	Temperature (°C)
1	11.5
2	12.5
3	13.3
4	13.9
5	14.3
6	14.7
7	15.2
8	15.6
9	15.9
10	16.4
Average	14.3

Based on these results, the average maximum temperature in the center of the pipe

was 14.3 °C . Given that the temperature at the center of the pipe only increased by 4.3 °C,

37

there was no significant radial conduction into the nitrogen gas. Additionally, heat appears to collect at the end of the pipe (arc length = 5 m), which was due to the nitrogen gas carrying the heat to the top of the pipe and thermal insulation that existed at the top of the pipe. As the sintering process continued, the temperature at the center of the pipe continued to increase. However, the average maximum temperature remained well below the required 45 °C maximum.

Figure 3.4.1-2 below describes the temperature at the center of the pipe for all time steps with the nitrogen gas flow turned "off". The maximum temperature at the center of the pipe for each heater with the associated average are described below in Table 3.4.1-2.
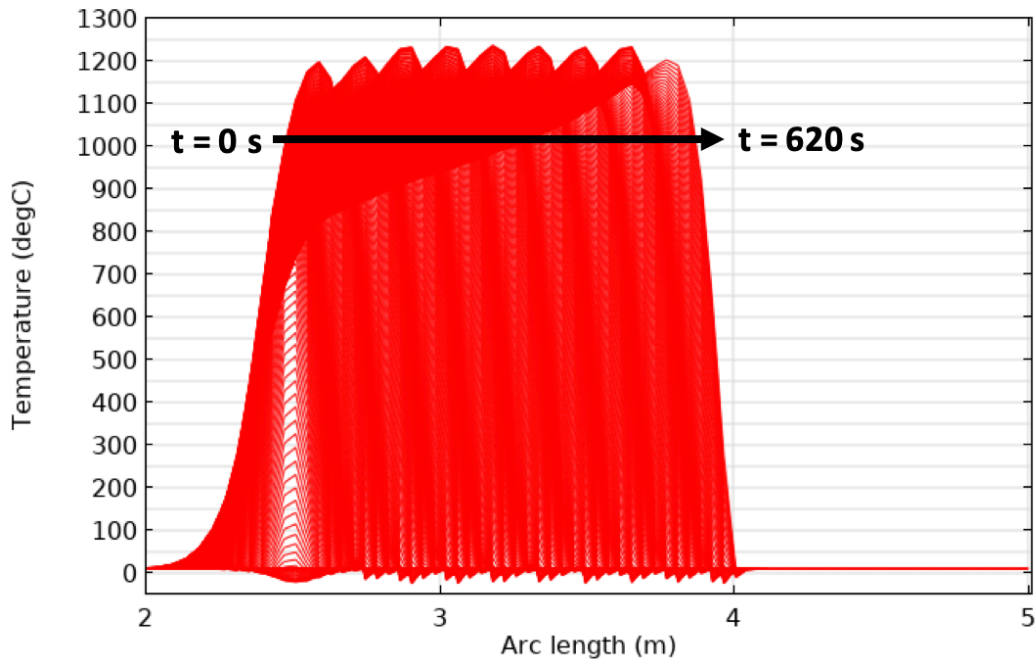
Figure 3.4.1-2: Temperature of the center of the pipe with nitrogen gas flow "off" for all heaters. Each line represents the temperature at the center of the pipe at a specific axial length for each second of the simulation from 0 s to 620 s. Each peak represents the maximum temperature that an individual heater reaches at the center of the pipe. Note that only the peaks for Heaters 2 – 10 are shown. The peak for Heater 1 is "hidden" within the peak for Heater 2.

Table 3.4.1-2: Maximum temperature at the center of the pipe (with nitrogen gas flow "off") for each heater with the associated average.

Heater	Temperature (°C)
1	1014
2	1199
3	1210
4	1233
5	1234
6	1237
7	1235
8	1233
9	1234
10	1203
Average	1203

Without a flow of nitrogen gas, the temperature at the center of the pipe reached an average maximum of 1203 °C. This high temperature, which was much greater than the maximum allowable temperature of 45 °C, would damage the integrity of the robotic tools in the pipe. These results indicate that a cooling agent was necessary to keep the center of the pipe below 45 °C, and nitrogen gas was an effective cooling agent.

3.4.2. Nitrogen Gas/Paste Boundary

Figure 3.4.2-1 below illustrates the temperature at the nitrogen gas/paste boundary for all time steps. The maximum temperature at the nitrogen gas/paste boundary with the associated average are described below in Table 3.4.2-1.
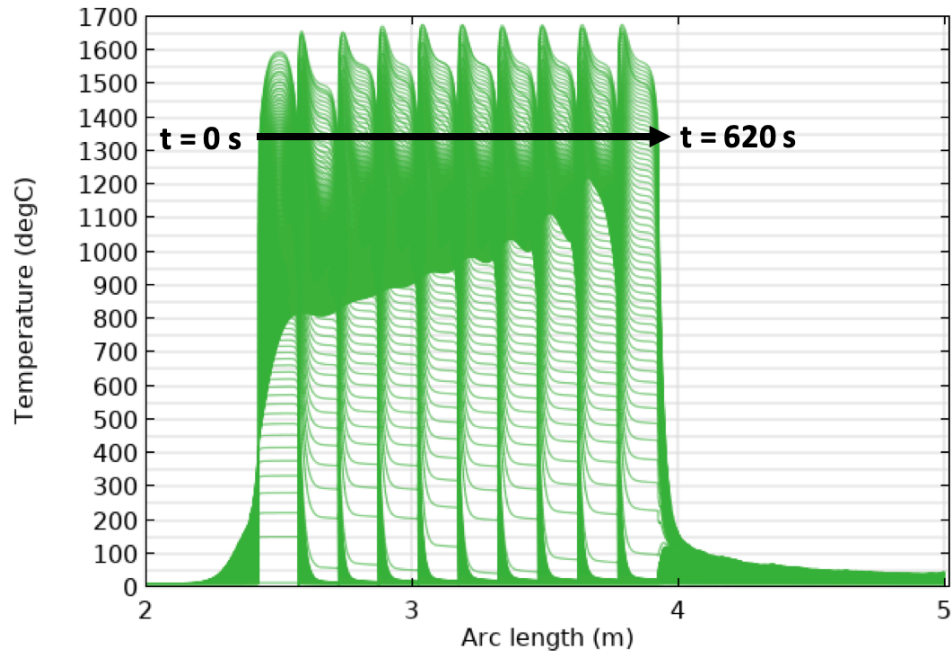
Figure 3.4.2-1: Nitrogen gas/paste boundary temperatures for all heaters. Each line represents the temperature at the nitrogen gas/paste boundary temperature at a specific axial length for each second of the simulation from 0 s to 620 s. Each peak represents the maximum temperature that an individual heater reaches at the nitrogen gas/paste boundary.

Table 3.4.2-1: Maximum temperature at the nitrogen gas/paste boundary for each heater with the associated average.

Heater	Temperature (°C)
1	1596
2	1657
3	1655
4	1673
5	1677
6	1677
7	1675
8	1676
9	1676
10	1677
Average	1664

These results indicate that the average maximum temperature at the nitrogen gas/paste boundary was 1664 °C. At all points in the sintering process, the temperature at the nitrogen gas/paste boundary exceeded the minimum required temperature of 1400 °C, suggesting that the paste was fully sintered at this boundary.

3.4.3. Paste/Pipe Boundary

Figure 3.4.3-1 below illustrates the temperature at the paste/pipe boundary for all time steps. The maximum temperature at the paste/pipe boundary with the associated average are described below in Table 3.4.3-1.
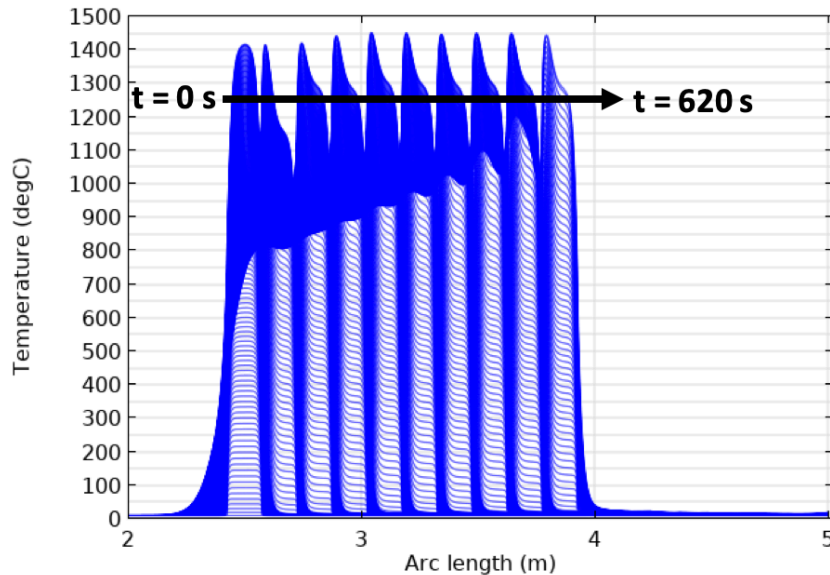
Figure 3.4.3-1: Paste/pipe boundary temperature for all heaters. Each line represents the temperature at the paste/pipe boundary temperature at a specific axial length for each second of the simulation from 0 s to 620 s. Each peak represents the maximum temperature that an individual heater reaches at the paste/pipe boundary.

Table 3.4.3-1: Maximum temperature at the paste/pipe boundary for each heater with the associated average.

Heater	Temperature (°C)
1	1416
2	1415
3	1421
4	1442
5	1452
6	1451
7	1448
8	1451
9	1450
10	1445
Average	1439

These results show that the average maximum temperature at the paste/pipe boundary was 1439 °C. At all points in the sintering process, the temperature at the nitrogen gas/paste boundary exceeded the minimum required temperature of 1400 °C, suggesting that the paste was fully sintered at this boundary.

3.4.4. Radial Temperature Gradients

When comparing the average maximum temperature results from the nitrogen gas/paste and paste/pipe boundary, the radial temperature gradient was 225 °C. While both the nitrogen gas/paste and paste/pipe boundaries reached the target temperature of 1400 °C, the sintering process was not very uniform in the radial direction. In reality, the surface of the paste that was closer to the heat source would sinter first. Since the nitrogen gas/paste boundary had heat directly applied to it, that boundary temperature was raised more quickly than the paste/pipe boundary. A more uniform sintered paste layer would require a smaller temperature gradient. To decrease the temperature gradient, the focus should be placed on

decreasing the temperature at the nitrogen gas/paste boundary because the temperature at this boundary exceeded the target temperature by 264 °C. Furthermore, the time component (sintering time) must be taken into account when assessing the sintering process. Even though the temperature requirement was met, the time requirement must also be met for successful sintering.

3.4.5. Pipe/Soil Boundary

Figure 3.4.5-1 below depicts the temperature at the pipe/soil boundary for all time steps. The maximum temperature at the pipe/soil boundary with the associated average are described below in Table 3.4.5-1.
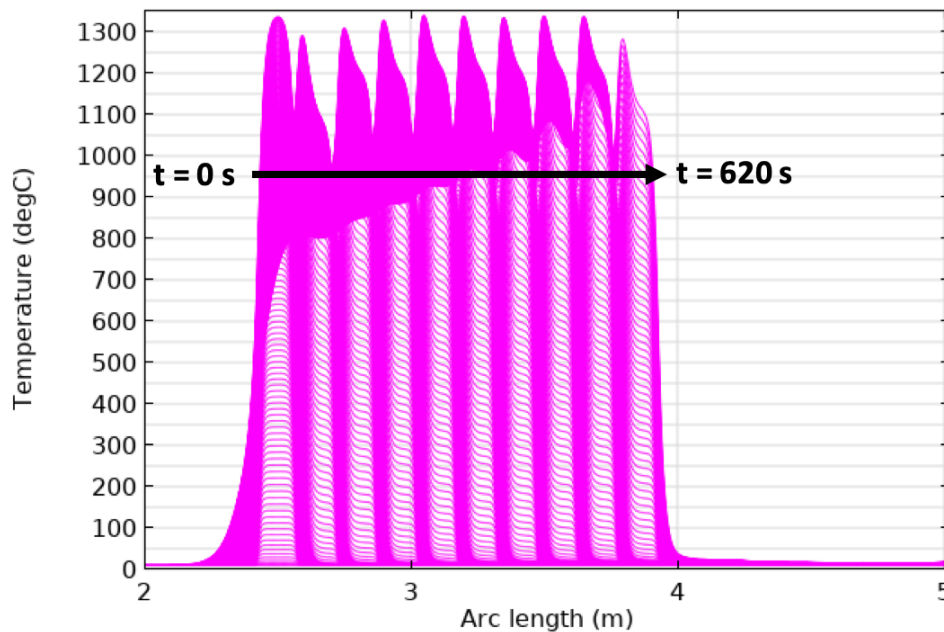
Figure 3.4.5-1: Pipe/soil boundary temperature for all heaters. Each line represents the temperature at the pipe/soil boundary at a specific axial length for each second of the simulation from 0 s to 620 s. Each peak represents the maximum temperature that an individual heater reaches at the pipe/soil boundary.

43

Table 3.4.5-1: Maximum temperature at the pipe/soil boundary for each heater with the associated average.

Heater	Temperature (°C)
1	1336
2	1291
3	1309
4	1328
5	1340
6	1338
7	1334
8	1338
9	1337
10	1283
Average	1323

These results show that the average maximum temperature at the pipe/soil boundary was 1323 °C. This suggests that the heat from the sintering process was transferred from the paste, through the pipe, and to the soil since the original temperature of this interface was 10 °C. The temperature at the pipe/soil boundary exceeded 100 °C at various points in the sintering process, suggesting that ground water could potentially boil off at this interface. This could pose some environmental and/or safety concerns.

3.5. Radial Temperature Profile Results

The purpose of analyzing the radial cut-line temperature profiles was to determine the axial temperature gradients in the paste and to determine how far heat dissipated into the soil in the radial direction. To analyze the temperature profiles from the radial cut-lines, the maximum temperature at the beginning, middle, and end of the pipe (in the axial direction) was plotted to the nearest 1 °C in the COMSOL plots. Please note that the curves present in Figure 3.5.1-1 – Figure 3.5.2-2 vary in smoothness due to the different meshing

in each domain. The curves between arc length = 0.129 m to 0.141 m have a higher smoothness than curves outside of this region due to the high-resolution mesh area. Additionally, please note that temperature peaks exist in the nitrogen gas domain in Figure 3.5.1-1, Figure 3.5.1-2, Figure 3.5.2-1, and Figure 3.5.2-2. This was due to an anomaly that pinned the temperature of a heater at 10 °C (the initial temperature) until the heater was turned "on". This anomaly may be due to how COMSOL implemented the initial temperature conditions into the heat transfer modules, but further research will be conducted on the specific causes of this anomaly. Moreover, the locations of the top, center, and bottom of the heater, which are relevant to the radial cut-line results, are defined below in Figure 3.5-1.
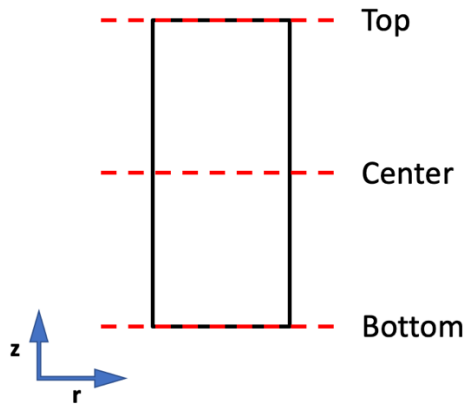
Figure 3.5-1: Location of the top, center, and bottom of a heater.

3.5.1. Center of the Heater

To analyze the temperature profile at the beginning of the pipe, the temperature profile was analyzed after Heater 1 had been "on" for the full sintering time of 85 seconds. Figure 3.5.1-1 below describes the radial temperature profiles for all heaters after 85 seconds.
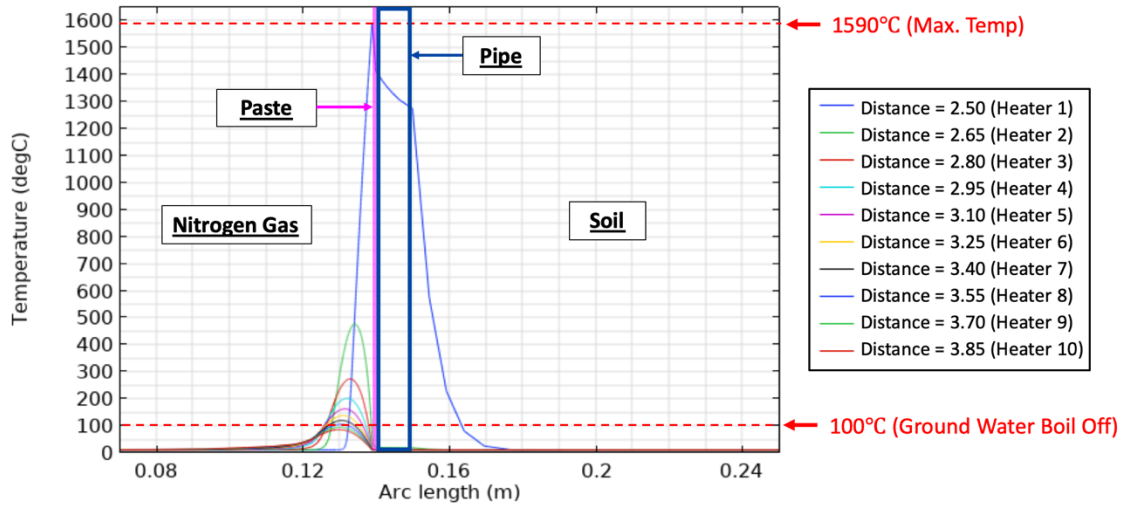
Figure 3.5.1-1: Temperature profiles for the radial cut-lines through the center of each heater after 85 seconds.

Based on these results, the maximum temperature was 1590℃, which was due to Heater 1. This maximum temperature occurred at the nitrogen gas/paste boundary. Even though Heater 1 was the only heater that was turned "on", all of the other heaters were well above the initial temperature of 10 °C. These results indicate that heat was not centralized to the heater that was turned "on". Instead, nitrogen gas carried heat up the pipe while power was being applied to the heater that was "on". Additionally, at 16.4 cm, which was 1.4 cm into the soil, the soil exceeded 100 °C, raising the concern of ground water boil off.

To analyze the temperature profile at the middle of the pipe, the temperature profile was analyzed after Heater 5 had been "on" for the full sintering time of 60 seconds. Figure 3.5.1-2 below describes the radial temperature profiles for all heaters after 320 seconds.
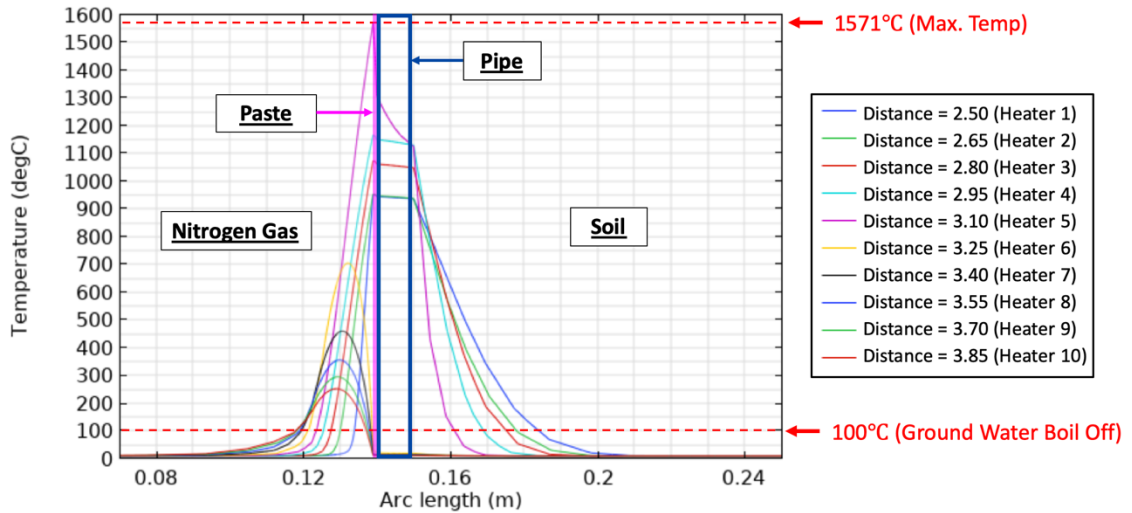
Figure 3.5.1-2: Temperature profiles for the radial cut-lines through the center of each heater after 320 seconds.

These results indicate that the maximum temperature was 1571°C, which was due to Heater 5. This maximum temperature occurred at the nitrogen gas/paste boundary. A steep temperature gradient in the paste was present for the heater that was "on" (Heater 5) while all previous heaters (Heaters 1 – 4) had minimum temperature gradients in the paste. Condution of heat continued from the nitrogen gas/paste boundary, through the paste, through the pipe, and finally to the soil. Heat traveled even further into the soil domain when comapred to the results when Heater 1 was "on". The soil exceeded 100 °C, the point of ground water boil off, at 18.4 cm, which was 3.4 cm into the soil.

To analyze the temperature profile at the end of the pipe, the temperature profile was analyzed after Heater 10 had been "on" for the full sintering time of 60 seconds. Figure 3.5.1-3 below describes the radial temperature profiles for all heaters after 620 seconds.
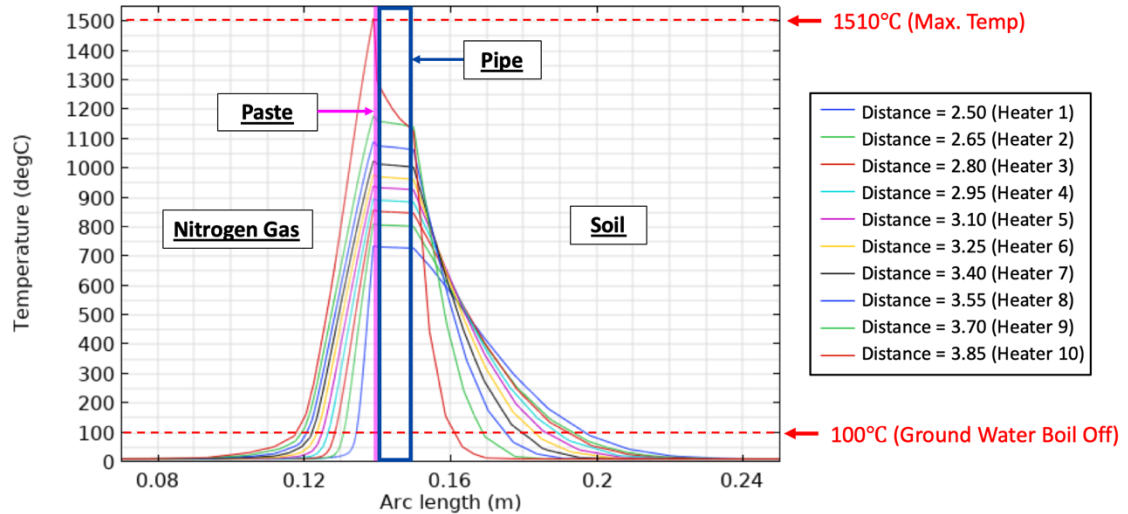
Figure 3.5.1-3: Temperature profiles for the radial cut-lines through the center of each heater after 620 seconds.

Based on these results, the maximum temperature was 1510 °C, which was due to Heater 10. This maximum temperature occurred at the nitrogen gas/paste boundary. At the end of the pipe, the previous heaters had not cooled back to the initial temperature of 10 °C. Even 535 seconds after Heater 1 was turned "off", Heater 1 only cooled to 736 °C, which was an 854 °C decrease from when Heater 1 was turned "off". Heater 1 remained well above the initial temperature of 10 °C. Furthermore, heat still propagated through the soil as the sintering process continued due to the continuation of heat that was applied to the nitrogen gas/paste boundary. At 19.7 cm, which was 4.7 cm into the soil, the soil exceeded 100 °C, raising the concern of ground water boil off.

3.5.2. Boundary of the Heater

The temperature at the boundary between the heaters was assessed to determine the axial temperature gradient within Heater 5. Temperatures were read from the nitrogen gas/paste boundary, and the temperature within the soil was not assessed. To analyze the

48

axial temperature gradient in Heater 5, the temperature profile was examined after Heater 5 had been "on" for the full sintering time of 60 seconds. Figure 3.5.2-1 below describes the radial temperature profiles through the boundary of each heater for all heaters after 320 seconds.
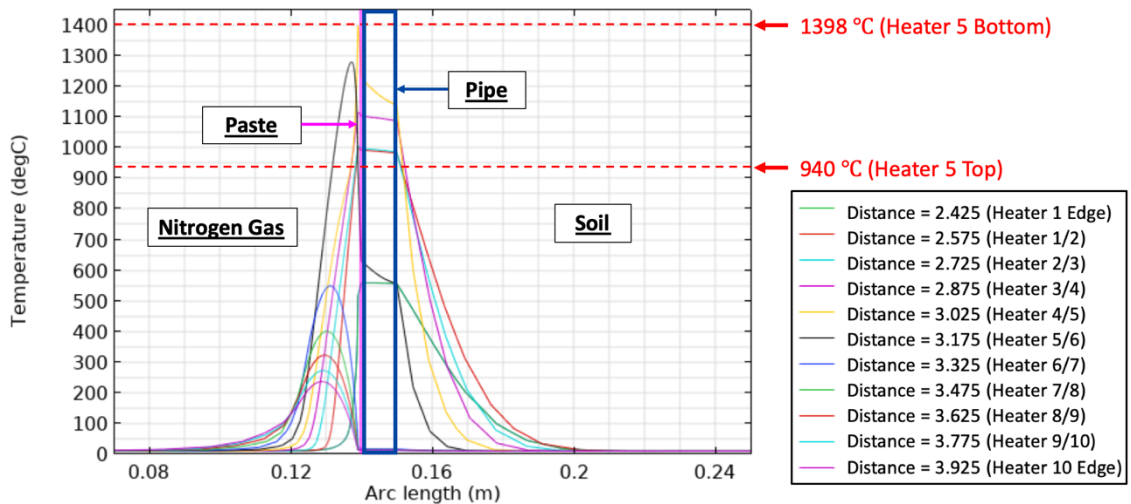
Figure 3.5.2-1: Temperature profiles for the radial cut-lines through the boundary of each heater after 320 seconds.

Figure 3.5.2-1 shows that the top of Heater 5 reached 940 °C while the bottom of Heater 5 reached 1398 °C. The bottom of Heater 5 reached a higher temperature than the top due to the residual heat that was present after Heater 4 had completed sintering. The heat from Heater 4 was transferred to the bottom of Heater 5, raising the temperature of the bottom of Heater 5.

To determine the maximum temperature of the top of Heater 5, the temperature profile was examined after Heater 6 had been "on" for the full sintering time of 60 seconds. Figure 3.5.2-2 below describes the radial temperature profiles through the boundary of each heater for all heaters after 380 seconds.

49
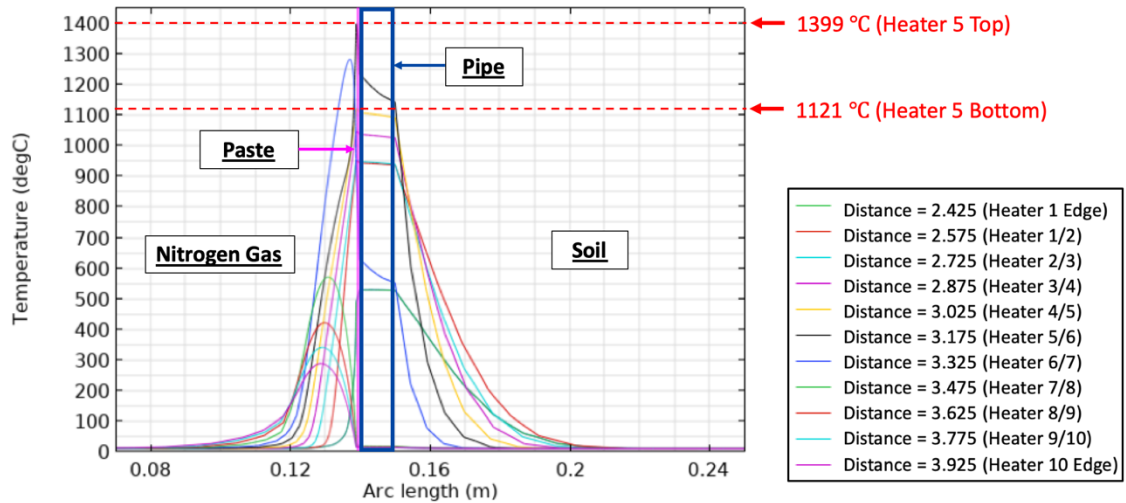
Figure 3.5.2-2: Temperature profiles for the radial cut-lines through the boundary of each heater after 380 seconds.

Figure 3.5.2-2 shows that the top of Heater 5 reached 1399 °C while the bottom of Heater 5 reached 1121 °C. The top of Heater 5 reached a higher temperature than the bottom due to the residual heat that was present after Heater 6 had completed sintering. The heat from Heater 6 was transferred to the top of Heater 5, raising the temperature of the top of Heater 5.

3.5.3. Axial Temperature Gradients

The radial cut-lines provided a useful visual for temperature gradient analysis within Heater 5. The temperature gradients at the lower half of the heater (Bottom/Center), top half of the heater (Center/Top), and throughout the heater (Bottom/Top) was assessed. The results, which are presented below in Table 3.5.3-1, were assessed at the maximum temperatures at the top, center, and bottom of Heater 5.

Table 3.5.3-1: Axial temperature gradient of Heater 5

Temperature (°C) at Each Axial Location in Heater 5			Temperature Gradient (°C)		
Bottom	**Center**	**Top**	**Bottom/Center**	**Center/Top**	**Bottom/Top**
1398	1571	1399	173	172	1

The results indicate that heat generation was centralized at the middle of the heater. For Heater 5, the center of the heater reached a higher temperature than the edges (bottom and top), showing that the paste was not uniformly sintered in the axial direction. The higher temperature at the center of Heater 5 created the larger bottom/center and center/top temperature gradients. The low bottom/top temperature gradient indicates that the edges of the heater received similar amounts of heat.

3.6 Energy Efficiency

The energy efficiency of Heater 1 was assessed to determine the fraction of heat that remained in the paste during the sintering process. The final power, P_{out}, for Heater 1 was determined at the sintering time, ST, of Heater 1 using Eq. 12 below in Table 3.6-1. The density, ρ, heat capacity, C_p, and final temperature, T_{final}, of the paste were calculated at 85 seconds. T_{final} was the average temperature throughout the paste where Heater 1 was applied, which was determined using a domain probe in COMSOL. The volume, V_{paste}, of the paste was the annular volume of the section of paste where Heater 1 was applied. V_{paste} was calculated using the outer radius of the paste, R_{outer}, the inner radius of the paste, R_{inner}, and the length of the heater, Lh. The efficiency, η, was determined using Eq. 13 below in Table 3.6-1 with the input power, P_{in}, as the total applied power for Heater 1. All variables

are summarized below in Table 3.6-2. Ultimately, the efficiency of Heater 1 was determined to be ~ 64%.

Table 3.6-1: Efficiency equations summary table

Equation Group #	Equation
12	$P_{out} = \dfrac{\rho_{paste} V_{paste} C_{p,paste} (T_{final} - T_{initial})}{ST_1 \cdot 1000}$ $V_{paste} = \pi \cdot \left(R_{paste,o}^2 - R_{paste,i}^2\right) \cdot Lh$
13	$\eta = \dfrac{P_{out}}{P_{in}} \cdot 100\%$

Table 3.6-2: Summary table for all variables used in the equations in Table 3.6-1 above.

Notation	Value	Unit
ρ_{paste}	6400	kg/m^3
$C_{p,paste}$	9136	J/kg·°C
T_{final}	1419	°C
$T_{initial}$	10	°C
ST	85	s
$R_{paste,o}$	0.14	m
$R_{paste,i}$	0.139	m
Lh	0.15	m
V_{paste}	1.315·10^{-4}	m^3
P_{out}	127.431	kW
P_{in}	200	kW
η	63.715	%

Chapter 4: Conclusion

4.1. Results Summary

Based on the optimized parameters, Heater 1 received 200 kW for 85 seconds, Heater 2 received 250 kW for 55 seconds, and Heaters 3 – 10 received 250 kW for 60 seconds. The surface of the paste on the interior of the pipe reached an average maximum of 1664 °C, while the paste surface adjacent to the pipe reached 1439 °C, resulting in an average radial temperature gradient of 225°C within the paste. Various temperature gradients also existed axially in the paste. We can assume that our model solutions are accurate based on the mesh quality and convergence study results. The convergence study results also indicate a trade-off that existed between the error and solver time, with a lower error resulting in higher solver time. While the steel paste exceeded the minimum target temperature of 1400 °C, full sintering within 30 seconds was unachievable. Further work on identifying the roles of conduction, convection, and radiation would lead to a more accurate sintering model.

4.2. Potential Concerns

While the optimized set of parameters resulted in nitrogen gas/paste and paste/pipe boundaries that reached a minimum of 1400 °C, there are still several potential concerns with the sintering process. One such concern is that the sintering process was too slow. The optimized parameters did not meet the necessary requirement of 15 m/hr. In fact, the

average linear speed was only 9 m/hr. The sintering time for the heaters must be decreased to achieve the ideal sintering rate and make the process useful within the time constraints. Additionally, temperature gradients existed axially and radially in the pipe, showing that the paste was not unfirmly sintered in either direction. This could potentially impact the structural integrity of the final sintered paste layer due to varying residual stresses that result from the thermal gradients.

Regarding environmental impacts, ground water boil off could pose an issue. The temperature of the soil immediately on the exterior of the pipe was above the boiling point of water (100 °C). However, the temperature exceeded 100 °C only a few centimeters into the soil. Therefore, the concern of ground water boil off would most likely be minimal, especially because the original pipe is buried under several meters of soil. Moreover, radiation, which is an important heat transfer mechanism that is involved in sintering, was not considered in this model. The lack of radiation could have impacted the accuracy of our model and is an important area for future work.

4.3. Recommendations & Future Work

The exact method of heat application and orientation of the heater should be carefully defined based on further experimental work to increase the accuracy of the model. Currently, heating only occurs in the axial direction with a sequential heating method. However, other heating methods are possible. For example, heating could occur as a function of theta and z such that heat moves along the inner circumference of the pipe and travels axially up the pipe. "Moving mesh" and "Pulse Heating" are additional methods

that could be utilized to produce a transient heating model. Furthermore, future models should aim to further quantify and improve the heater efficiency by implementing methods to contain more of the heat within the paste and prevent heat from dissipating into the environment.

Large temperature gradients in the radial direction, which affect the uniformity of the final sintered product, could be combated with pulse heating. A short burst of high heat could be applied to the nitrogen gas/paste boundary with enough time for the heat to travel to the paste/pipe boundary before delivering another burst of heat. This method would allow the temperature of the paste/pipe boundary to catch up to the nitrogen gas/paste boundary, resulting in a lower radial temperature gradient. A reduced heater length in the axial direction could also potentially help to decrease the temperature gradients in the axial direction.

Further research should be conducted on welding processes in a pipeline environment, and welding typically includes radiation as a heat transfer mechanism. Given that radiation was not considered in this model, the effects of radiation should be studied in future models. The radiative properties of the paste must be determined so that the radiative heat transfer modules in COMSOL can be used. These modules would allow reflectance, absorbance, and transmittance due to radiation to be better accounted for. When using the radiative heat transfer modules, the new parameters would be sintering time and sintering temperature (instead of applied power). These new parameters would align more closely with the literature.

Additional information on the material properties needs to be gathered to increase the accuracy of the model. Currently, the thermal conductivity of the paste prior to the phase change does not vary with temperature, and the soil properties are approximations. Material properties as a function of temperature produce more accurate results than material properties at a single temperature. The maximum allowable temperature of the paste should also be determined so that the maximum allowable temperature gradients can be assessed. Furthermore, the physical properties of the paste should be analyzed both during and post sintering. Residual stress could result from temperature variations during the sintering process, and the physical properties of the paste could change at such high temperatures.

Since this study focused on analyzing the sintering process of the initial 1 mm layer of paste, the remaining 2 mm of paste must still be sintered to the initial 1 mm. Additional methods and optimization will be required to sinter the remaining layers of paste. The model for the initial 1 mm paste layer should be updated to reflect these recommendations, which could then be applied to the remaining 2 mm of paste. Finally, a full convergence study on the entire pipeline environment should be performed instead of focusing on the nitrogen gas/paste boundary.

Appendices

Appendix A: Data collected on the SS316 properties by the University of Pittsburgh Wei Xiong Group

A.1 SS316 Density as a Function of Temperature

Temperature [K]	Calculated Density [g/cm^3]	Temperature [K]	Calculated Density [g/cm^3]
300	7.87	910	7.74
310	7.87	920	7.74
320	7.87	930	7.74
330	7.86	940	7.73
340	7.86	950	7.73
350	7.86	960	7.72
360	7.86	970	7.72
370	7.85	980	7.71
380	7.85	990	7.71
390	7.85	1000	7.70
400	7.84	1010	7.70
410	7.84	1020	7.70
420	7.84	1030	7.69
430	7.83	1040	7.69
440	7.83	1050	7.68
450	7.83	1060	7.68
460	7.82	1063.57	7.68
470	7.82	1063.57	7.68
480	7.81	1063.57	7.68
490	7.81	1070	7.67
500	7.81	1080	7.67
510	7.80	1090	7.66
520	7.80	1100	7.66
530	7.79	1110	7.65
540	7.79	1119.08	7.65
550	7.78	1119.08	7.65
560	7.78	1120	7.65
570	7.77	1120.86	7.65

580	7.77	1120.86	7.65
580	7.77	1120.86	7.65
590	7.76	1130	7.65
600	7.76	1140	7.64
604.81	7.75	1150	7.64
604.81	7.75	1160	7.63
610	7.75	1170	7.63
620	7.74	1180	7.62
623.17	7.74	1183.08	7.62
623.17	7.74	1183.08	7.62
623.17	7.74	1183.08	7.62
630	7.74	1190	7.62
640	7.74	1200	7.61
650	7.73	1210	7.61
660	7.73	1220	7.61
670	7.73	1230	7.60
680	7.72	1240	7.60
690	7.72	1250	7.59
700	7.72	1260	7.59
710	7.72	1270	7.58
720	7.72	1280	7.58
730	7.72	1290	7.57
740	7.71	1300	7.57
750	7.71	1310	7.57
760	7.71	1320	7.56
770	7.71	1330	7.56
780	7.71	1340	7.55
785.61	7.71	1350	7.55
785.61	7.71	1358.74	7.54
785.61	7.71	1358.74	7.54
790	7.72	1360	7.54
800	7.72	1370	7.54
810	7.72	1380	7.53
820	7.72	1390	7.53
830	7.72	1400	7.52
840	7.73	1410	7.52
850	7.73	1420	7.51
860	7.74	1430	7.51

870	7.74	1440	7.51
880	7.75	1450	7.50
890	7.75	1460	7.50
893.59	7.75	1470	7.49
893.59	7.75	1480	7.49
893.59	7.75	1490	7.48
900	7.75	1500	7.48

A.2 SS316 Heat Capacity as a Function of Temperature

Note that the heat capacity for Temperature = 10 °C was calculated from an external source.[18]

Temperature [°C]	Specific Heat Capacity [J/(mol-K)]	Temperature [°C]	Specific Heat Capacity [J/(mol-K)]
10.00[18]	27.12	906.85	39.76
299.85	41.66	911.85	40.13
304.85	42.33	916.85	40.50
309.85	43.04	921.85	40.89
314.85	43.78	926.85	41.28
319.85	44.56	931.85	41.67
324.85	45.39	936.85	42.07
329.85	46.26	941.85	42.47
334.85	47.20	946.85	42.88
339.85	48.19	951.85	43.29
344.85	49.27	956.85	43.70
349.85	50.43	961.85	44.11
354.85	51.70	966.85	44.51
359.85	53.11	971.85	44.92
364.85	54.71	976.85	45.33
369.85	56.55	981.85	45.74
374.52	58.60	986.85	46.14
376.69	50.87	991.85	46.55
379.85	51.51	996.85	46.95
384.85	52.80	1001.85	47.35
389.85	54.54	1006.85	38.53
394.85	56.96	1011.85	38.68
398.68	45.66	1016.85	38.83
399.85	45.72	1021.85	38.98
404.85	45.98	1026.85	39.13
409.85	46.25	1031.85	39.28
414.85	48.04	1036.85	39.42
419.85	46.80	1041.82	36.70
424.85	47.07	1041.85	35.27
429.85	47.35	1046.85	35.32

434.85	47.62	1051.85	35.38
439.85	47.89	1056.85	35.43
444.85	48.17	1061.85	35.48
449.85	48.45	1066.85	35.54
454.85	48.72	1071.85	35.59
459.85	49.02	1076.85	35.64
464.85	49.33	1081.85	35.70
469.85	49.64	1086.85	35.75
474.85	49.98	1091.85	35.80
479.85	50.33	1096.85	35.86
484.85	50.70	1101.85	35.91
489.85	51.10	1106.85	35.97
494.85	51.52	1111.85	36.02
499.85	51.98	1116.85	36.08
504.85	52.45	1121.85	36.13
505.85	52.55	1126.85	36.18
506.85	52.86	1131.85	36.24
511.85	53.17	1136.85	36.29
516.85	53.71	1141.85	36.35
521.85	54.28	1146.85	36.40
526.85	54.88	1151.85	36.46
531.85	55.49	1156.85	36.51
536.85	56.12	1161.85	36.57
541.85	56.77	1166.85	36.62
546.85	57.44	1171.85	36.68
551.85	58.11	1176.85	36.74
556.85	58.78	1181.85	36.79
561.85	59.45	1186.85	36.85
566.85	60.10	1191.85	36.90
571.85	60.74	1196.85	36.96
576.85	61.35	1201.85	37.01
581.85	61.92	1206.85	37.07
586.85	62.44	1211.85	37.13
591.85	62.88	1216.85	37.18
596.81	36.23	1221.85	37.24
596.85	36.23	1226.85	37.30
601.85	36.31	1231.85	37.35
606.85	36.40	1236.85	37.41

611.85	36.49	1241.85	37.47
616.85	36.57	1246.85	37.52
621.85	36.66	1251.85	37.58
626.85	36.75	1256.85	37.64
631.85	36.84	1261.85	37.70
636.85	36.93	1266.85	37.76
641.85	37.01	1271.85	37.82
646.85	37.10	1276.85	37.88
651.85	37.19	1281.85	37.94
656.85	37.28	1286.85	38.00
661.85	37.37	1291.85	38.06
666.85	37.46	1296.85	38.11
671.85	37.55	1301.85	38.17
676.85	37.64	1306.85	38.23
681.85	37.73	1311.85	38.29
686.85	37.83	1316.85	38.35
691.85	37.93	1321.85	38.41
696.85	38.03	1326.85	38.47
699.47	37.44	1331.85	38.53
701.85	37.56	1336.85	38.59
706.85	37.82	1341.85	38.65
711.85	38.08	1346.85	38.71
716.85	38.34	1348.02	38.72
721.85	38.61	1351.85	48.31
726.85	38.88	1356.85	51.76
731.85	39.15	1361.85	56.50
736.85	39.43	1366.85	63.06
741.85	39.70	1371.85	72.23
746.85	39.99	1376.85	85.08
751.85	40.27	1381.85	103.13
756.85	40.56	1386.85	128.40
761.85	40.85	1391.85	163.62
766.85	41.14	1393.82	180.95
771.85	41.44	1396.85	212.71
776.85	41.74	1399.06	230.57
781.85	42.04	1401.85	220.73
784.58	42.20	1406.85	281.52
785.35	36.48	1411.85	360.57

785.35	34.84	1416.85	459.48
786.85	36.52	1420.84	547.67
791.85	36.67	1420.84	528.50
794.44	38.42	1421.85	571.74
796.85	34.69	1423.86	62.91
801.85	34.86	1423.86	42.58
806.85	35.04	1426.85	42.64
811.85	35.22	1431.85	42.74
816.85	35.41	1436.85	42.85
821.85	35.61	1441.85	42.96
826.85	35.82	1446.85	43.06
831.85	36.03	1451.85	43.17
833.92	34.68	1456.85	43.28
833.92	35.46	1461.85	43.37
836.85	35.59	1466.85	43.47
841.85	35.82	1471.85	43.57
846.85	36.06	1476.85	43.66
851.85	36.31	1481.85	43.76
856.85	36.57	1486.85	43.86
861.85	36.84	1491.85	43.96
866.85	37.12	1496.85	44.06
871.85	37.42	1501.85	44.16
876.85	37.72	1506.85	44.26
881.85	38.03	1511.85	44.37
886.85	38.36	1516.85	44.47
891.85	38.70	1521.85	44.57
896.85	39.04	1526.85	44.68
901.85	39.39	10000.00	44.68

A.3 SS316 Solid Fraction Graph
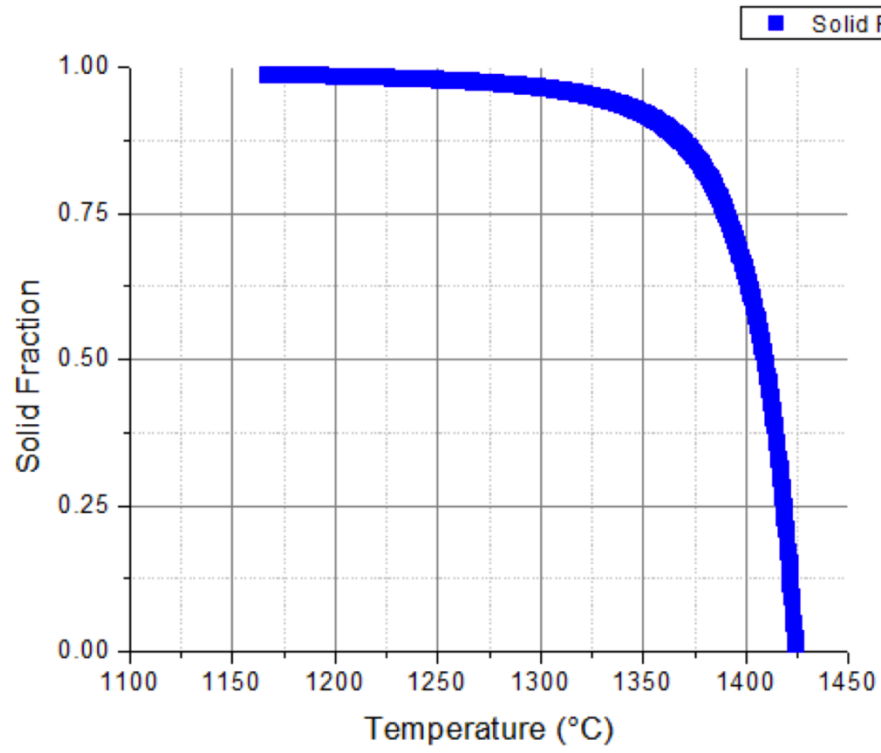
A.4 SS316 Latent Heat as a Function of Temperature

Temperature [°C]	Latent Heat [J/mol]	Temperature [°C]	Latent Heat [J/mol]
1423.85	-7.40	1293.55	-15777.13
1423.35	-314.70	1293.05	-15794.39
1422.85	-611.93	1292.55	-15811.61
1422.35	-899.93	1292.05	-15828.79
1421.85	-1179.07	1291.55	-15845.93
1421.35	-1449.71	1291.05	-15863.03
1421.02	-1626.30	1290.55	-15880.09
1420.52	-1885.80	1290.05	-15897.11
1420.02	-2138.19	1289.55	-15914.09
1419.52	-2383.05	1289.05	-15931.03
1419.02	-2620.65	1288.55	-15947.93
1418.52	-2851.30	1288.05	-15964.80
1418.02	-3075.28	1287.55	-15981.63
1417.52	-3292.83	1287.05	-15998.42
1417.02	-3504.22	1286.55	-16015.18
1416.52	-3709.68	1286.05	-16031.90
1416.02	-3909.44	1285.55	-16048.58
1415.52	-4103.72	1285.05	-16065.23
1415.02	-4292.73	1284.55	-16081.84
1414.52	-4476.66	1284.05	-16098.42
1414.02	-4655.71	1283.55	-16114.97
1413.52	-4830.05	1283.05	-16131.49
1413.02	-4999.86	1282.55	-16147.97
1412.52	-5165.30	1282.05	-16164.41
1412.02	-5326.53	1281.55	-16180.83
1411.52	-5483.71	1281.05	-16197.22
1411.02	-5636.97	1280.55	-16213.57
1410.52	-5786.45	1280.05	-16229.89
1410.02	-5932.29	1279.55	-16246.18
1409.52	-6074.62	1279.05	-16262.44
1409.02	-6213.55	1278.55	-16278.68
1408.52	-6349.21	1278.05	-16294.88
1408.02	-6481.69	1277.55	-16311.05
1407.52	-6611.12	1277.05	-16327.20
1407.02	-6737.60	1276.55	-16343.31
1406.52	-6861.21	1276.05	-16359.40
1406.02	-6982.06	1275.55	-16375.46
1405.52	-7100.24	1275.05	-16391.50
1405.02	-7215.84	1274.55	-16407.51
1404.52	-7328.93	1274.05	-16423.49
1404.02	-7439.61	1273.55	-16439.44
1403.52	-7547.94	1273.05	-16455.37

1403.02	-7654.00	1272.55	-16471.28
1402.52	-7757.86	1272.05	-16487.16
1402.02	-7859.59	1271.55	-16503.01
1401.52	-7959.27	1271.05	-16518.84
1401.02	-8056.94	1270.55	-16534.65
1400.52	-8152.67	1270.05	-16550.44
1400.02	-8246.53	1269.55	-16566.20
1399.52	-8338.56	1269.05	-16581.94
1399.02	-8428.83	1268.55	-16597.65
1398.52	-8517.39	1268.05	-16613.35
1398.02	-8604.28	1267.55	-16629.02
1397.52	-8689.55	1267.05	-16644.67
1397.02	-8773.26	1266.55	-16660.30
1396.52	-8855.45	1266.05	-16675.91
1396.02	-8936.16	1265.55	-16691.50
1395.52	-9015.43	1265.05	-16707.07
1395.02	-9093.31	1264.55	-16722.63
1394.52	-9169.84	1264.05	-16738.16
1394.02	-9245.05	1263.55	-16753.67
1393.55	-9314.23	1263.05	-16769.17
1393.05	-9395.74	1262.55	-16784.65
1392.55	-9476.87	1262.05	-16800.11
1392.05	-9556.66	1261.55	-16815.55
1391.55	-9634.98	1261.05	-16830.98
1391.05	-9711.82	1260.55	-16846.39
1390.55	-9787.23	1260.05	-16861.78
1390.05	-9861.25	1259.55	-16877.16
1389.55	-9933.91	1259.05	-16892.52
1389.05	-10005.26	1258.55	-16907.87
1388.55	-10075.34	1258.05	-16923.21
1388.05	-10144.18	1257.55	-16938.53
1387.55	-10211.82	1257.05	-16953.83
1387.05	-10278.29	1256.55	-16969.13
1386.55	-10343.63	1256.05	-16984.41
1386.05	-10407.86	1255.55	-16999.68
1385.55	-10471.02	1255.05	-17014.93
1385.05	-10533.15	1254.55	-17030.18
1384.55	-10594.26	1254.05	-17045.41
1384.05	-10654.39	1253.55	-17060.63
1383.55	-10713.56	1253.05	-17075.84
1383.05	-10771.80	1252.55	-17091.04
1382.55	-10829.13	1252.05	-17106.23
1382.05	-10885.58	1251.55	-17121.42
1381.55	-10941.17	1251.05	-17136.59
1381.05	-10995.93	1250.55	-17151.76
1380.55	-11049.88	1250.05	-17166.91

1380.05	-11103.03	1249.55	-17182.06
1379.55	-11155.41	1249.05	-17197.20
1379.05	-11207.04	1248.55	-17212.34
1378.55	-11257.94	1248.05	-17227.47
1378.05	-11308.12	1247.55	-17242.59
1377.55	-11357.61	1247.05	-17257.71
1377.05	-11406.42	1246.55	-17272.82
1376.55	-11454.58	1246.05	-17287.93
1376.05	-11502.08	1245.55	-17303.04
1375.55	-11548.96	1245.05	-17318.14
1375.05	-11595.23	1244.55	-17333.24
1374.55	-11640.90	1244.05	-17348.34
1374.05	-11685.99	1243.55	-17363.43
1373.55	-11730.50	1243.05	-17378.52
1373.05	-11774.47	1242.55	-17393.61
1372.55	-11817.89	1242.05	-17408.70
1372.05	-11860.78	1241.55	-17423.79
1371.55	-11903.15	1241.05	-17438.88
1371.05	-11945.03	1240.55	-17453.98
1370.55	-11986.40	1240.05	-17469.07
1370.05	-12027.30	1239.55	-17484.16
1369.55	-12067.73	1239.05	-17499.26
1369.05	-12107.70	1238.55	-17514.36
1368.55	-12147.22	1238.05	-17529.46
1368.05	-12186.30	1237.55	-17544.57
1367.55	-12224.96	1237.05	-17559.68
1367.05	-12263.19	1236.55	-17574.80
1366.55	-12301.02	1236.05	-17589.93
1366.05	-12338.45	1235.55	-17605.06
1365.55	-12375.48	1235.05	-17620.19
1365.05	-12412.13	1234.55	-17635.34
1364.55	-12448.41	1234.05	-17650.49
1364.05	-12484.32	1233.55	-17665.65
1363.55	-12519.87	1233.05	-17680.82
1363.05	-12555.08	1232.55	-17696.00
1362.55	-12589.94	1232.05	-17711.19
1362.05	-12624.46	1231.55	-17726.39
1361.55	-12658.65	1231.05	-17741.61
1361.05	-12692.53	1230.55	-17756.83
1360.55	-12726.08	1230.05	-17772.07
1360.05	-12759.33	1229.55	-17787.32
1359.55	-12792.28	1229.05	-17802.59
1359.05	-12824.93	1228.55	-17817.87
1358.55	-12857.29	1228.05	-17833.17
1358.05	-12889.37	1227.55	-17848.49
1357.55	-12921.17	1227.05	-17863.82

1357.05	-12952.69	1226.55	-17879.17
1356.55	-12983.95	1226.05	-17894.54
1356.05	-13014.95	1225.55	-17909.93
1355.55	-13045.69	1225.05	-17925.34
1355.05	-13076.18	1224.55	-17940.77
1354.55	-13106.42	1224.05	-17956.22
1354.05	-13136.42	1223.55	-17971.69
1353.55	-13166.18	1223.05	-17987.19
1353.05	-13195.71	1222.55	-18002.71
1352.55	-13225.01	1222.05	-18018.26
1352.05	-13254.08	1221.55	-18033.83
1351.55	-13282.94	1221.05	-18049.43
1351.05	-13311.58	1220.55	-18065.06
1350.55	-13340.01	1220.05	-18080.72
1350.05	-13368.23	1219.55	-18096.40
1349.55	-13396.25	1219.05	-18112.12
1349.05	-13424.07	1218.55	-18127.86
1348.55	-13451.69	1218.05	-18143.64
1348.05	-13479.12	1217.55	-18159.45
1347.55	-13506.36	1217.05	-18175.30
1347.05	-13533.41	1216.55	-18191.18
1346.55	-13560.28	1216.05	-18207.10
1346.05	-13586.97	1215.55	-18223.05
1345.55	-13613.48	1215.05	-18239.04
1345.05	-13639.82	1214.55	-18255.07
1344.55	-13665.99	1214.05	-18271.14
1344.05	-13691.99	1213.55	-18287.25
1343.55	-13717.83	1213.05	-18303.41
1343.05	-13743.51	1212.55	-18319.60
1342.55	-13769.02	1212.05	-18335.84
1342.05	-13794.38	1211.55	-18352.13
1341.55	-13819.59	1211.05	-18368.46
1341.05	-13844.65	1210.55	-18384.84
1340.55	-13869.55	1210.05	-18401.27
1340.05	-13894.32	1209.55	-18417.75
1339.55	-13918.93	1209.05	-18434.28
1339.05	-13943.41	1208.55	-18450.86
1338.55	-13967.75	1208.05	-18467.49
1338.05	-13991.95	1207.55	-18484.18
1337.55	-14016.01	1207.05	-18500.93
1337.05	-14039.94	1206.55	-18517.73
1336.55	-14063.75	1206.05	-18534.59
1336.05	-14087.42	1205.55	-18551.51
1335.55	-14110.97	1205.05	-18568.49
1335.05	-14134.39	1204.55	-18585.53
1334.55	-14157.69	1204.05	-18602.64

1334.05	-14180.87	1203.55	-18619.81
1333.55	-14203.93	1203.05	-18637.05
1333.05	-14226.88	1202.55	-18654.35
1332.55	-14249.70	1202.05	-18671.72
1332.05	-14272.42	1201.55	-18689.17
1331.55	-14295.02	1201.05	-18706.68
1331.05	-14317.52	1200.55	-18724.27
1330.55	-14339.90	1200.05	-18741.93
1330.05	-14362.18	1199.55	-18759.67
1329.55	-14384.35	1199.05	-18777.48
1329.05	-14406.42	1198.55	-18795.37
1328.55	-14428.39	1198.05	-18813.34
1328.05	-14450.25	1197.55	-18831.39
1327.55	-14472.02	1197.05	-18849.53
1327.05	-14493.69	1196.55	-18867.74
1326.55	-14515.26	1196.05	-18886.04
1326.05	-14536.73	1195.55	-18904.43
1325.55	-14558.12	1195.05	-18922.91
1325.05	-14579.41	1194.55	-18941.47
1324.55	-14600.60	1194.05	-18960.13
1324.05	-14621.71	1193.55	-18978.87
1323.55	-14642.73	1193.05	-18997.71
1323.05	-14663.66	1192.55	-19016.65
1322.55	-14684.51	1192.05	-19035.68
1322.05	-14705.27	1191.55	-19054.80
1321.55	-14725.94	1191.05	-19074.03
1321.05	-14746.53	1190.55	-19093.35
1320.55	-14767.04	1190.05	-19112.78
1320.05	-14787.47	1189.55	-19132.31
1319.55	-14807.82	1189.44	-19137.82
1319.05	-14828.09	1189.43	-19137.74
1318.55	-14848.29	1189.35	-19141.37
1318.05	-14868.40	1189.33	-19141.82
1317.55	-14888.44	1189.28	-19144.00
1317.05	-14908.41	1189.24	-19145.68
1316.55	-14928.30	1188.74	-19169.11
1316.05	-14948.12	1188.24	-19194.00
1315.55	-14967.87	1187.74	-19218.74
1315.05	-14987.54	1187.24	-19243.20
1314.55	-15007.15	1186.74	-19267.47
1314.05	-15026.68	1186.24	-19291.63
1313.55	-15046.15	1185.74	-19315.72
1313.05	-15065.55	1185.24	-19339.79
1312.55	-15084.88	1184.74	-19363.86
1312.05	-15104.15	1184.24	-19387.93
1311.55	-15123.35	1183.74	-19412.02

1311.05	-15142.49	1183.24	-19436.13
1310.55	-15161.57	1182.74	-19460.27
1310.05	-15180.58	1182.24	-19484.43
1309.55	-15199.53	1181.74	-19508.63
1309.05	-15218.41	1181.24	-19532.85
1308.55	-15237.24	1180.74	-19557.10
1308.05	-15256.01	1180.24	-19581.38
1307.55	-15274.72	1179.74	-19605.69
1307.05	-15293.37	1179.24	-19630.03
1306.55	-15311.96	1178.74	-19654.40
1306.05	-15330.49	1178.24	-19678.80
1305.55	-15348.97	1177.74	-19703.23
1305.05	-15367.40	1177.40	-19719.87
1304.55	-15385.76	1176.90	-19743.30
1304.05	-15404.08	1176.40	-19761.61
1303.55	-15422.34	1175.90	-19777.18
1303.05	-15440.54	1175.40	-19791.16
1302.55	-15458.70	1174.90	-19804.15
1302.05	-15476.80	1174.40	-19816.46
1301.55	-15494.85	1173.90	-19828.27
1301.05	-15512.85	1173.40	-19839.72
1300.55	-15530.80	1172.90	-19850.87
1300.05	-15548.70	1172.40	-19861.79
1299.55	-15566.55	1171.90	-19872.52
1299.05	-15584.35	1171.40	-19883.10
1298.55	-15602.11	1170.90	-19893.56
1298.05	-15619.81	1170.40	-19903.90
1297.55	-15637.47	1169.90	-19914.16
1297.05	-15655.09	1169.40	-19924.35
1296.55	-15672.65	1168.90	-19934.47
1296.05	-15690.18	1168.40	-19944.53
1295.55	-15707.66	1167.90	-19954.54
1295.05	-15725.09	1167.40	-19964.51
1294.55	-15742.48	1166.90	-19974.44
1294.05	-15759.83	1166.40	-19984.33

Bibliography

[1] Rapid Encapsulation of Pipelines Avoiding Intensive Replacement (REPAIR); DE-FOA-0002289. *ARPA-E* (*Advanced Research Projects Agency-Energy)* **2020**. https://arpa-e-foa.energy.gov/FileContent.aspx?FileID=0ffe1347-e217-49a8-a666-15b9064592e4.

[2] Nath, N. K.; Al Awadhi, I.; Narayanan, S. Best Practices and Challenges for Pipeline Design and Construction in Populated Area. *Abu Dhabi International Petroleum Exhibition & Conference* **2016**. https://doi.org/10.2118/183101-MS.

[3] Lewnard, J. REPAIR Workshop Overview. *ARPA-E* (*Advanced Research Projects Agency-Energy)* **2019**. https://arpa-e.energy.gov/sites/default/files/Lewnard_REPAIR%20Workshop%20Overview%20Day%201_JL%20final.pdf.

[4] Wang, C.; Ping, W.; Bai, Q.; Cui, H.; Hensleigh, R.; Wang, R.; Brozena, A. H.; Xu, Z.; Dai, J.; Pei, Y.; Zheng, C.; Pastel, G.; Gao, J.; Wang, X.; Wang, H.; Zhao, J.-C.; Yang, B.; Zheng, X. (Rayne); Luo, J.; Mo, Y.; Dunn, B.; Hu, L. A General Method to Synthesize and Sinter Bulk Ceramics in Seconds. *Science* **2020**, *368* (6490), 521–526. https://doi.org/10.1126/science.aaz7681.

[5] Wang, C.; Ping, W.; Bai, Q.; Cui, H.; Hensleigh, R.; Wang, R.; Brozena, A. H.; Xu, Z.; Dai, J.; Pei, Y.; Zheng, C.; Pastel, G.; Gao, J.; Wang, X.; Wang, H.; Zhao, J.-C.; Yang, B.; Zheng, X. (Rayne); Luo, J.; Mo, Y.; Dunn, B.; Hu, L. Supplementary Materials for A General Method to Synthesize and Sinter Bulk Ceramics in Seconds. *Science* **2020**, *368* (6490), 521. https://science.sciencemag.org/content/sci/suppl/2020/04/29/368.6490.521.DC1/aaz7681_Wang_SM.pdf.

[6] Wang, C.; Zhong, W.; Ping, W.; Lin, Z.; Wang, R.; Dai, J.; Guo, M.; Xiong, W.; Zhao, J.-C.; Hu, L. Rapid Synthesis and Sintering of Metals from Powders. *Advanced Science* **2021**, 2004229. https://doi.org/10.1002/advs.202004229.

[7] Sanchez, A.; Ojeda, M.; Gomez, H.; Bermejo, C.; Medina, V.; Escorcia, O.; Bris, J.; Morelo, A.; Maury, H.; Medina, J. Review and Analysis of Repair/Rehabilitation Methods for Natural Gas Pipelines. *International Mechanical Engineering Congress and Exposition* **2017**. https://doi.org/10.1115/IMECE2017-71543.

[8] A. F. M. Arif, Y. N. Al-Nassar, H. Al-Qahtani, S. M. a. Khan, M. Anis, a. M. Eleiche, M. Inam, N. I. Al-Nasri, and H. M. Al-Muslim. Optimization of Pipe Repair Sleeve Design. *Journal of Pressure Vessel Technology* **2012.** 134(5): 051702. https://doi-org.proxy-um.researchport.umd.edu/10.1115/1.4006126.

[9] Najafi, M. Pipeline Rehabilitation Systems for Service Life extension (in Service Life Estimation and Extension of Civil Engineering Structures). *Woodhead Publishing* **2011**, 262–289.

[10] K. Farrag. Selection of Pipe Repair Methods; Final Rep. GTI Proj. Number 21087. *GTI (Gas Technology Institute)* **2013**.

[11] Orrù, R.; Licheri, R.; Locci, A. M.; Cincotti, A.; Cao, G. Consolidation/Synthesis of Materials by Electric Current Activated/Assisted Sintering. *Materials Science and Engineering: R: Reports* **2009**, *63* (4), 127–287. https://doi.org/10.1016/j.mser.2008.09.003.

[12] Manière, C.; Lee, G.; Olevsky, E. A. All-Materials-Inclusive Flash Spark Plasma Sintering. *Scientific Reports* **2017**, *7* (1), 15071. https://doi.org/10.1038/s41598-017-15365-x.

[13] Yao, Y.; Huang, Z.; Xie, P.; Lacey, S. D.; Jacob, R. J.; Xie, H.; Chen, F.; Nie, A.; Pu, T.; Rehwoldt, M.; Yu, D.; Zachariah, M. R.; Wang, C.; Shahbazian-Yassar, R.; Li, J.; Hu, L. Carbothermal Shock Synthesis of High-Entropy-Alloy Nanoparticles. *Science* **2018**, *359* (6383), 1489–1494. https://doi.org/10.1126/science.aan5412.

[14] Manière, C.; Lee, G.; Zahrah, T.; Olevsky, E. A. Microwave Flash Sintering of Metal Powders: From Experimental Evidence to Multiphysics Simulation. *Acta Materialia* **2018**, *147*, 24–34. https://doi.org/10.1016/j.actamat.2018.01.017.

[15] Hu, L.; Albertus, P.; Xiong, W.; Wang, C.; Petit de Mange, E.; Otgonbaatar, U. Pipe-in-Pipe by Rapid, Continuous, Smart Alloy Coating. *ARPA-E* (*Advanced Research Projects Agency-Energy*) **2021**, 2. https://arpa-e.energy.gov/sites/default/files/2021-01/Liangbing_Day%202.pdf.

[16] Properties of Various Ideal Gases (at 300 K). *Ohio University*. https://www.ohio.edu/mechanical/thermo/property_tables/gas/idealGas.html (accessed Apr 23, 2021).

[17] Wei Xiong Group, University of Pittsburgh, Pittsburgh, PA 15260, USA

[18] Stainless Steel - Grade 316 (UNS S31600). *AZO Materials*. https://www.azom.com/properties.aspx?ArticleID=863 (accessed Apr 23, 2021).

[19] Xie, X.; Li, D.; Tsai, T.-H.; Liu, J.; Braun, P. V.; Cahill, D. G. Thermal Conductivity, Heat Capacity, and Elastic Constants of Water-Soluble Polymers and Polymer Blends. *Macromolecules* **2016**, *49* (3), 972–978. https://doi.org/10.1021/acs.macromol.5b02477.

[20] PVP. *Polymer Database* **2017**.
http://polymerdatabase.com/polymers/polyvinylpyrrolidone.html (accessed Apr 23, 2021).

[21] Chen, Z. X.; Guo, X. X.; Shao, L. T.; Li, S. Q. On Determination Method of Thermal Conductivity of Soil Solid Material. *Soils and Foundations* **2020**, *60* (1), 218–228. https://www.sciencedirect.com/science/article/pii/S0038080620320424.

[22] Specific Heat of some common Substances. *Engineering ToolBox* **2003**. https://www.engineeringtoolbox.com/specific-heat-capacity-d_391.html (accessed Apr 23, 2021).

[23] Heat Transfer Module User's Guide for COMSOL Multiphysics v. 5.4. *COMSOL AB* **2018.** https://doc.comsol.com/5.4/doc/com.comsol.help.heat/HeatTransferModuleUsersGuide.pdf.

[24] Detailed Explanation of the Finite Element Method (FEM). *Multiphysics Cyclopedia* **2017**. https://www.comsol.com/multiphysics/finite-element-method.